EIDESSTATTLICHE ERKLÄRUNG

Ich erkläre an Eides statt, dass ich die vorliegende Arbeit selbstständig verfasst, andere als die angegebenen Quellen/Hilfsmittel nicht benutzt, und die den benutzten Quellen wörtlich und inhaltlich entnommenen Stellen als solche kenntlich gemacht habe. Das in TUGRAZonline hochgeladene Textdokument ist mit der vorliegenden Masterarbeit identisch.

_____   _____
            Datum   Unterschrift

Acknowledgement

This work would not have been possible without the support of so many special people. At this point, I would therefore like to take the opportunity to acknowledge people who contributed to the accomplishment of this master's thesis.

First of all, I would like to express my sincere gratitude to my supervisor Prof. Isabel Heidegger-Pircher for giving me the opportunity to work on this research project and for the great support and encouragement throughout this work. Moreover, I would like to specially thank Prof. Helmut Klocker, head of the Research Laboratory, Department of Urology, for the highly appreciated scientific advice in good times as in bad.

I would like to extend my thanks to all members of the Urology lab for the great time and the pleasant, stimulating work environment. Special thanks go to Andrea Eigentler for introducing me to everyday lab life and supporting me technically, and to Julia Höfer for the constructive and encouraging discussions, which were anything but granted.

Furthermore, I want to acknowledge Prof. Harald Pichler for providing the valuable distance supervision from my home university, the Graz University of Technology.

My heartfelt thanks go to my better half for being so proud of me and always believing in me!

Last but not least, I wish to thank my family from the bottom of my heart for the unconditional love, encouragement and support throughout my studies. Dear mom and dad, I never could have made it this far without you and I cannot thank you enough for all you have done and keep doing for me! This thesis is dedicated to you.

Thank you!

Abstract

Prostate cancer (PCa) is one of the most common cancers among men in developed countries. Evidence has accumulated exerting the importance of cullin-RING ubiquitin ligases (CRLs) and their regulator Cullin-associated NEDD8-dissociated protein 1 (Cand1) in various cancer entities. Thus, in the present study, we aimed to investigate the role of Cand1 in PCa.

Previously conducted next generation sequencing of PCa cell lines resistant to the anti-androgen enzalutamide revealed *cand1* being one out of five commonly mutated genes. Using a pool of four targeting siRNAs we hence downregulated Cand1 in the metastatic PCa cell lines. Thereby, knockdown of Cand1 significantly reduced cell viability and proliferation in LNCaP and PC3 cells and increased apoptosis. Similar effects were observed in enzalutamide resistant (EnzaR) cells, however, less pronounced compared to the respective treatment-naive cell lines. Besides downregulation, we optimised overexpression of Cand1 in PC3 cells by introducing the plasmid pCMV6-XL6-Cand1. Using immunofluorescence staining, we could confirm nuclear and cytoplasmic localisation of Cand1 in PCa cells. In addition, we interrogated the BioProfiling database for validation of expression in PCa, and found that low Cand1 expression is associated with increased overall survival in patients with localised PCa.

In summary, we demonstrated in this thesis that Cand1 modulates cell proliferation, viability and apoptotic behaviour of hormone-therapy-naive as well as enzalutamide resistant cell lines. Moreover, Cand1 levels seem to correlate with overall survival rates in PCa patients. Thus, we propose further investigations on Cand1 in order to reveal its impact on PCa progression and its potential involvement in enzalutamide resistance.

Zusammenfassung

Das Prostatakarzinom (PCa) ist eine der häufigsten Krebserkrankungen bei Männern in Industrieländern. Diverse Studien zeigten die Bedeutung von Cullin-RING-Ubiquitin-Ligasen (CRLs) und ihrem regulatorischen Protein, dem Cullin-assoziierten NEDD8-dissoziierten Protein 1 (Cand1) in verschiedenen Krebsentitäten. Das Ziel der vorliegenden Arbeit besteht darin, die Rolle von Cand1 beim PCa zu untersuchen.

In einer Vorstudie konnte mittels Next Generation Sequencing von PCa-Zelllinien, welche resistent gegen das Anti-Androgen Enzalutamid (EnzaR) sind, gezeigt werden, dass *cand1* eines von fünf gemeinsam mutierten Genen in EnzaR-Zellen ist. Unter Verwendung eines Pools von vier spezifischen siRNAs wurde daher die Expression von Cand1 in metastasierten PCa Zelllinien LNCaP und PC3, sowie in LAPC-4 EnzaR- und LNCaP abl EnzaR-Zellen runterreguliert. Der Knockdown von Cand1 bewirkte dabei eine signifikant verminderte Viabilität und Proliferation von LNCaP- und PC3- Zellen und führte im Gegenzug zu einer Zunahme der Apoptose. Ähnliche Effekte wurden in EnzaR-Zellen beobachtet, jedoch weniger ausgeprägt im Vergleich zu den unbehandelten Kontrollzellen. Mittels Immunfluoreszenz konnten wir eine nukleäre und zytoplasmatische Lokalisation von Cand1 in PCa-Zellen bestätigen. Außerdem konnten wir mithilfe der BioProfiling-Plattform zeigen, dass eine niedrige Cand1-Expression mit einem signifikant verlängerten Gesamtüberleben von Patienten mit lokal begrenztem PCa einhergeht.

Zusammenfassend konnten wir in dieser Arbeit zeigen, dass Cand1 die Zellproliferation, die Viabilität und das apoptotische Verhalten von Hormontherapie-naiven sowie Enzalutamid-resistenten Zellen beeinflusst. Darüber hinaus scheint das Cand1-Level mit den Gesamtüberlebensraten bei PCa-Patienten zu korrelieren. Nichtsdestotrotz sind weitere Studien zu Cand1 notwendig, um den Einfluss des Proteins auf die Progression des PCa und seine potenzielle Beteiligung an der Enzalutamid-Resistenz zu erforschen.

Contents

1 Introduction

1.1 Physiology, function and anatomy of the prostate

The prostate is a chestnut-sized, exocrine gland that is part of the male reproductive tract of mammals [1,2]. It produces a thin, milky, slightly acidic fluid which is released into the vas deferens during ejaculation accounting for 20 – 30% of the semen volume [3,4].

The prostatic fluid is enriched in citrate for pH maintenance, contains spermidine and spermine for the motility of spermatozoa, as well as prostaglandins which stimulate vaginal secretions and contraction of the uterus for fast transport of the sperms. Liquefaction of the semen is regulated by high levels of Zn^{2+} by modulating the activity of phosphatases and proteases in the prostatic fluid [3,5,6].

Macroscopically, the normal prostate is 3 cm long, 4 cm wide and 2 cm in depth and weighs about 20 g. It is located anterior to the rectum, right below the urinary bladder, where it surrounds the urethra (figure 1) [7].
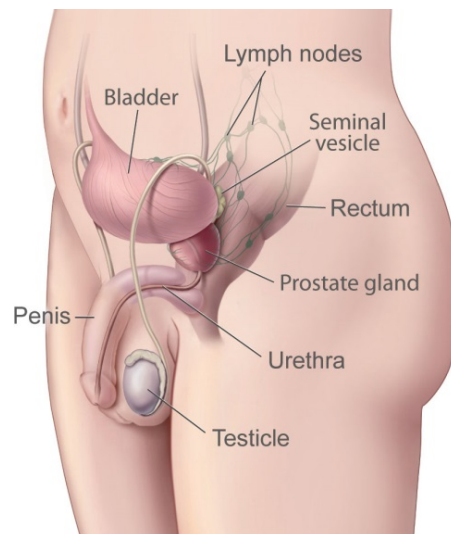
Figure 1: Side view of the human male reproductive and urinary anatomy.

Source: https://www.cancer.gov/types/prostate/understanding-prostate-changes [29/09/2017]

Microscopically, the prostate is composed of two main compartments, namely the exocrine glandular epithelium tissue (70%) and the fibromuscular stroma (30%) [6-8]. The glandular tissue is responsible for the production and secretion of prostatic fluid,

while the fibromuscular tissue contracts during ejaculation. This contraction facilitates expulsion of the semen and prevents urination during ejaculation [8].

In 1986, the pathologist John McNeal proposed the concept of anatomic zones of the human prostate [9,10]. The prostate can thus be divided into four major zones: transition zone, central zone, peripheral zone and anterior fibromuscular stroma (figure 2). The transition zone (5 to 10% of glandular tissue) is traversed by the proximal urethra, the central zone (25% of the glandular tissue) surrounds the ejaculatory ducts and the peripheral zone (70% of the glandular tissue) is perforated by the distal prostatic urethra (figure 2) [7,11].
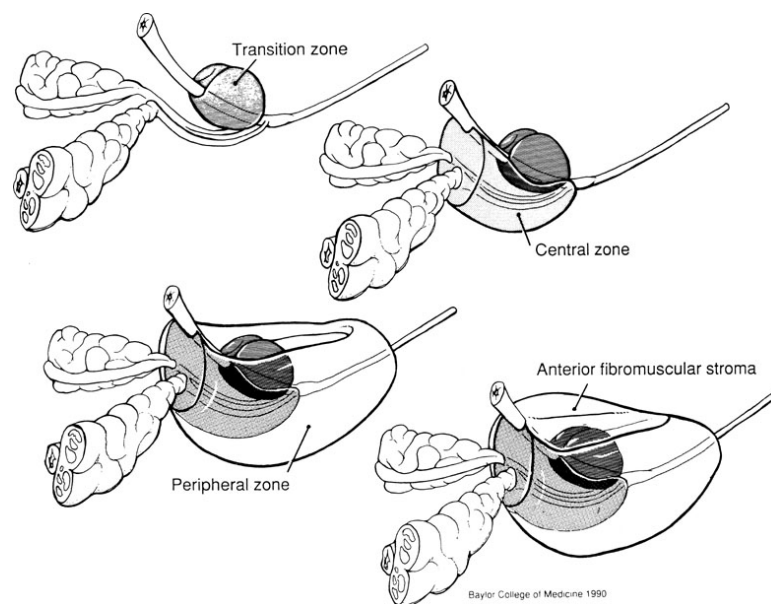
Figure 2: Anatomy of the prostate and zonal classification by McNeal.
Source: http://scgap.systemsbiology.net/figures/Prostate_Anatomy.php [02/09/2017]

1.2   Prostate cancer

1.2.1   Epidemiology and risk factors for prostate cancer

Prostate cancer (PCa) is one of the most common cancers in men worldwide with over one million newly diagnosed cases every year [12]. Recent statistical analyses from patients in the United States indicated that approximately 180,890 men were diagnosed with PCa in 2016, being thus the most common solid neoplasm in men of the United States [13]. Interestingly, PCa incidence is lower in Asia and Africa compared to Europe and America (figure 3) [14].
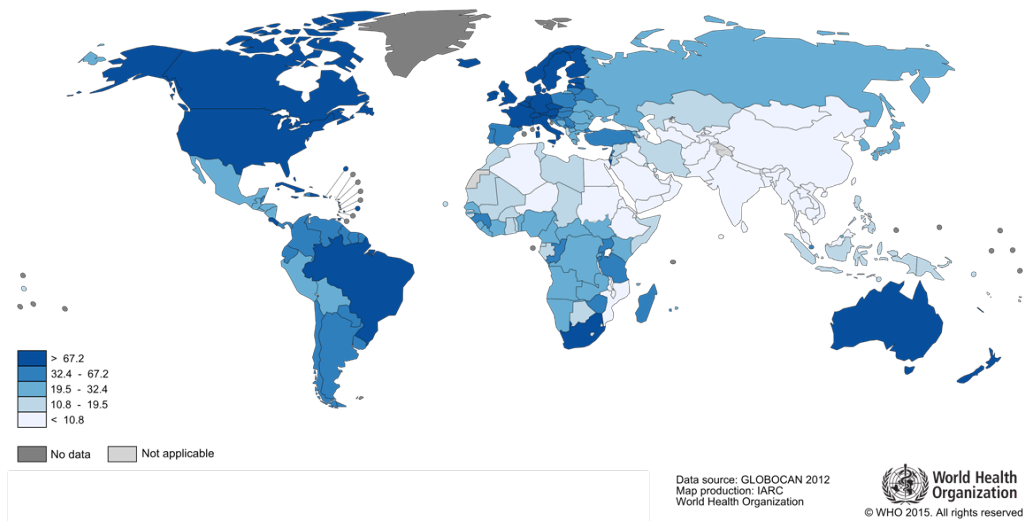
Figure 3: Estimated incidence rates of PCa per 100,000 worldwide in 2012.
Source: http://globocan.iarc.fr/old/FactSheets/cancers/prostate-new.asp [03/10/2017]

As for many other types of cancer, the exact cause for the development of PCa in men is not known. However, some well-established factors have been identified which increase the risk of the disease:

75% of PCa are diagnosed in men over the age of 65, mirroring the strong correlation between PCa incidence and *increasing age* [15,16]. Another important risk factor is *family history*. If one first-degree relative is diagnosed with PCa, the risk of developing the disease is doubled. It increases five to eleven-fold, if two or more first-degree relatives are affected. 9% of patients suffer from true hereditary PCa, meaning that three or more first-degree relatives are affected or not less than two were diagnosed with early onset disease before the age of 55 [16]. Furthermore, *genetic predisposition* may be involved in pathogenesis of the disease. Several studies have uncovered putative loci for hereditary PCa [17-19], observing that germline mutations in the *BRCA2* gene increase the risk of PCa. In addition, *BRCA1* and *BRCA2* mutations are associated with a more aggressive clinical course [20,21]. Moreover, androgen receptor (AR) mutations were suggested to play a role in PCa progression and might be involved in treatment resistance [22,23].

As mentioned above, the incidence of PCa differs among various geographical areas (figure 3), showing high rates in Northern America and Europe and low rates in Southeast Asia. This can partly be explained by *ethnicity*, another factor proven to correlate with PCa development [14]. However, migration studies give evidence for

an increased risk for PCa in Japanese and Chinese men when moving to the United States. Moreover, the risk of second generation Asian immigrants approaches that of American men [16]. These findings suggest that also exogenous factors like environment and lifestyle might be aetiologically important for PCa initiation and progression. There are also several studies investigating the impact of sexual behaviour, nutrition or chronic inflammation on the risk of PCa [16,24-28].

1.2.2   Development and progression of PCa

Histologically, 95% of prostatic malignancies are adenocarcinomas, of which 70% arise in the peripheral zone and 20% in the transition zone. Only 8% are found in the central zone; however, these tumours tend to show a more aggressive clinical course [7,29].

In general, initiation and progression of cancer is driven by the accumulation of genetic alterations which cause the inactivation of tumour suppressor genes and/or overexpression of oncogenes.

The schematic model in figure 4 illustrates the developmental pathway of human PCa, where the tumour develops from normal epithelium via prostatic intraepithelial neoplasia and adenocarcinoma to metastatic disease. Characteristic for the progression from one stage to the other is the loss of distinct chromosomal regions that harbour tumour suppressor genes encoding for example retinoblastoma (*RB*), phosphatase and tensin homologue (*PTEN*), or cell cycle inhibitors like p27 or p53 [30]. The main pathway involved in PCa initiation and progression is the AR signalling axis. In general, the AR is a nuclear transcription factor belonging to the steroid hormone receptor superfamily. In absence of androgens, the AR is located in the cytoplasm and bound by heat shock proteins. Upon ligand binding, the receptor undergoes conformational changes resulting in the dissociation of the chaperones and its interaction with co-regulators. These again facilitate the translocation of the AR into the nucleus, where it subsequently dimerises and stimulates the transcription of androgen responsive genes such as the prostate-specific antigen (PSA), or genes involved in cell growth and survival like CCND1 encoding cyclin D1 and EAF2, the ELL-associated factor 2 [31,32]. The

androgen signalling plays thus a pivotal role in both, the normal development and function of the prostate, as well as in its pathological growth [33-35].
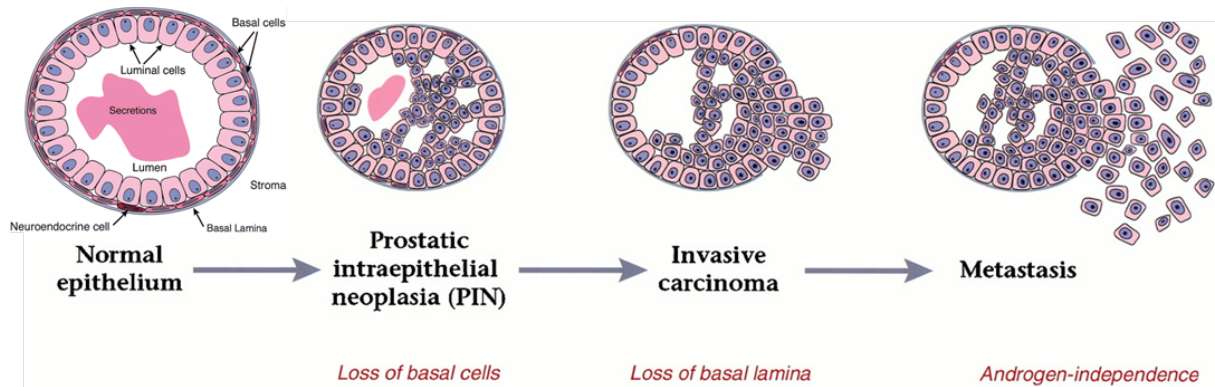
Figure 4: Development of human prostate cancer.

Source: [30]

1.2.3 Diagnosis of PCa

Locally advanced or metastatic PCa is often associated with weight loss, fatigue and irritative urinary voiding symptoms up to urinary retention. However, these symptoms are not characteristic for PCa, as primary organ-confined PCa is mostly asymptomatic. Therefore, early recognition is necessary in order to detect malignant transformations at an early and potentially treatable stage [16]. The main tools for diagnosing PCa include digital rectal examination (DRE) and/or measurement of PSA concentration in serum, leading to an ultrasonography- or magnetic resonance tomography (MRT)-based biopsy in case of suspicious findings.

Digital rectal examination (DRE). As described above, the majority of the PCa arises in the peripheral zone of the prostate which is located in close proximity to the rectum. Thus, PCa with volumes ≥ 0.2 mL can be palpated by the doctor's finger and possible malignancies further pathologically confirmed by biopsy. The sensitivity of this diagnostic examination lies around 40% [15,16].

Prostate-specific antigen (PSA). PSA, also known as kallikrein-3 (KLK-3) is a chymotrypsin-like serine protease which is secreted into the prostatic fluid by epithelial cells of the prostate. It is responsible for the cleavage of semenogelin I and II and therefore necessary for liquefaction of the semen and thus for the motility of spermatozoa [36]. Although PCa leads to elevated levels of PSA in the blood, it

cannot be termed a cancer-specific marker, as also non-malignant diseases like prostatitis and benign prostatic hyperplasia (BPH) show increased PSA levels [15,16]. As a consequence of the age-related increase of prostate size, the PSA level of men changes over the years. Therefore, standard PSA values for clinical diagnosis of PCa were adapted to the age of the patient. The following table lists PSA limits used in the Department of Urology at the Medical University of Innsbruck [37] (table 1).

Table 1: Age-specific reference ranges for serum PSA levels currently used at the Department of Urology at the Medical University of Innsbruck [37].

Age group	Serum PSA cut-off values
≤ 49 years	1.75 ng/mL
50 – 59 years	1.75 ng/mL
60 – 69 years	2.25 ng/mL
≥ 70 years	3.25 ng/mL

Prostate biopsy. Definitive diagnosis of PCa can only be confirmed histologically by biopsy of the prostate which can be performed ultrasonography- or MRT-guided, where at least ten needle biopsies of the prostate are taken for histopathological diagnosis [16].

1.2.4 Classification and histopathological grading of PCa

Elevated PSA levels and/or abnormalities found on DRE require biopsy and further histopathological analysis. If PCa is confirmed, it is crucial to define cancer size and spread as well as the degree of morphological changes. The most frequently used methods to classify patients are the TNM classification (stage) and the Gleason score (grade).

1.2.4.1 TNM classification of PCa

The TNM classification is the most widely used system for PCa staging. It is based on the extent of the primary *tumour* (T), the presence or absence of spread to regional lymph *nodes* (N) and the presence or absence of distant *metastasis* (M) [15]. The following table describes the stages of PCa according to the TNM system (table 2).

Table 2: TNM staging system.

TNM	Stage	Description
Tumour (T)	**TX**	Tumour cannot be assessed
	T0	No evidence of tumour
	T1	Clinically unapparent tumour not detected by physical exam (DRE) or visible by imaging
	T1a	Tumour found incidentally in tissue removed from prostate for other reasons, histologic finding in < 5% of tissue resected
	T1b	Tumour found incidentally in tissue removed from prostate for other reasons, histologic finding in > 5% of tissue resected
	T1c	Tumour identified by needle biopsy because of elevated PSA
	T2	Tumour confined within the prostate
	T2a	Tumour involves 50% of one lobe or less
	T2b	Tumour involves > 50% of one lobe but not both lobes
	T2c	Tumour involves both lobes
	T3	Tumour extends outside the prostate capsule
	T3a	Regional lymph nodes were not assessed
	T3b	No spread to nearby lymph nodes
	T4	Metastasis in nearby lymph node(s)
Regional Lymph Nodes (N)	**NX**	Distant metastasis cannot be assessed (not evaluated)
	N0	No distant metastasis
	N1	Distant metastasis
Distant Metastasis (M)	**MX**	Lymph node(s) outside of nearby area
	M0	Bone(s)
	M1	Other site(s) with or without bone disease
	M1a	Regional lymph nodes were not assessed
	M1b	No spread to nearby lymph nodes
	M1c	Metastasis in nearby lymph node(s)

Adapted according to:

http://www.urologyhealth.org/urologic-conditions/advanced-prostate-cancer/grading-and-staging

1.2.4.2 Gleason score

The Gleason grading system, first described by the pathologist Donald Gleason and his colleagues, is the standard histological grading method for carcinoma of the prostate [38]. The Gleason score is composed of two Gleason grades which are allocated in biopsy and surgical specimens. They describe the degree of differentiation and architecture of PCa cells of the most extensive (primary) pattern and the second most common (secondary) pattern. The grades can range from 1 to 5, with high values representing an increased deviation from the normal histological architecture of the prostate (figure 5) [39]. Summation of the two predominating grades yield in a Gleason score of minimum 2 and maximum 10, with 2 being the least aggressive and 10 the most aggressive tumour [38-40].
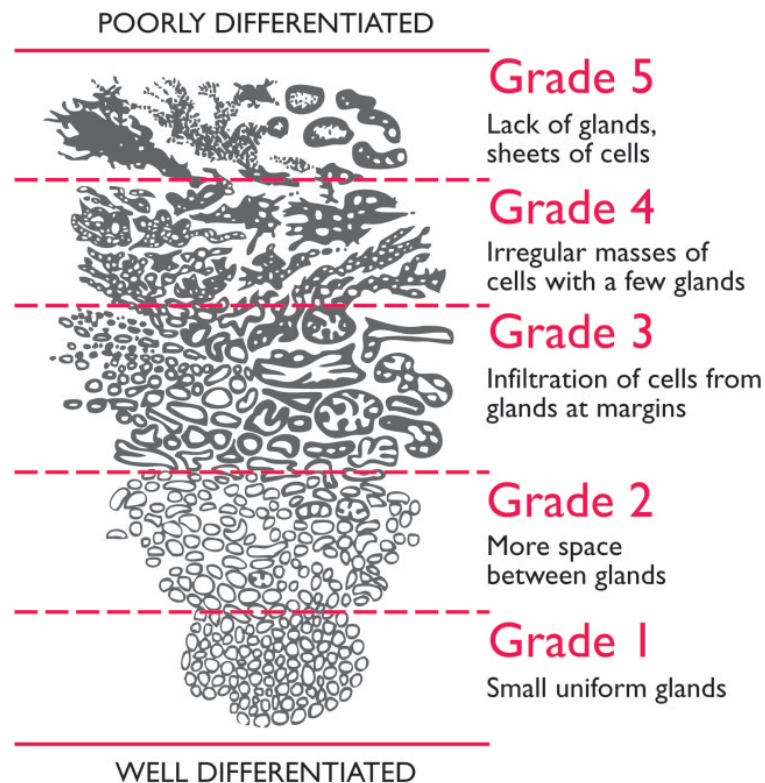

Figure 5: Histological determination of Gleason grades.
Source: https://orchid-cancer.org.uk/prostate-cancer/diagnosis-2/2000-2/ [09.10.2017]

1.2.4.3 ISUP classification

In order to align the PCa grading based on the above mentioned Gleason score with the grading of other carcinomas and to stratify patients for better prediction of clinical outcome, the International Society of Urological Pathology (ISUP) recently modified the Gleason score. Based on a proposal of researchers of the Johns Hopkins Medical Institutions, the ISUP agreed in 2014 on compressing Gleason scores ≤ 6 in prognostic grade group I, dividing Gleason score 7 into prognostic grade group II (prevalent Gleason grade 3, 3+4=7) and III (prevalent Gleason grade 4, 4+3=7), assigning Gleason score 8 to prognostic grade group IV and Gleason scores 9-10 to grade V [41,42].

1.2.5 Standard therapy options

There are several different treatment options available for PCa patients. The appropriate therapy, however, varies depending on tumour stage as well as age and physical and psychological constitution of the patient.

1.2.5.1 Treatment of organ-confined PCa

1.2.5.1.1 Active surveillance

In case of *active surveillance*, the patient is kept under close surveillance with three-monthly PSA measurements and re-biopsies once a year. If the PSA level rises above 10 ng/mL or histological changes are observed in re-biopsy, active therapy is started. This strategy is applied in order to achieve correct timing for curative treatment and to prevent over-treatment and unnecessary side effects [15].

1.2.5.1.2 Radical prostatectomy

In radical prostatectomy, the entire prostate gland and the two seminal vesicles are surgically removed [16].

1.2.5.1.3 Radiation therapy

In radiation therapy, focal high-energy irradiation is used to cause extensive DNA damage in cancer cells, which eventually leads to cell death. Concerning PCa, there are two main therapies: external beam radiation (EBRT) which aims from outside the body to the location of the tumour or internal radiation (brachytherapy) delivered through radioactive seeds implanted into the prostate [43].

1.2.5.2 Treatment of advanced and metastatic castration-resistant PCa

1.2.5.2.1 Hormone ablation therapy

As mentioned above, the prostate is a hormone-dependent organ and development and progression of PCa are driven by androgens [16]. Already in 1941, Huggins and Hodges provided evidence that androgen deprivation has positive effects on PCa growth, and hormone ablation has been standard therapy for advanced PCa for over 70 years now [44].

Suppression of testosterone levels can be achieved by surgical or chemical castration:

In *bilateral orchiectomy*, the hormone-producing testicles are surgically removed and castration levels are reached within 3-10 h [16].

Luteinizing hormone-releasing hormone (LHRH) agonists continuously stimulate LHRH receptors resulting in a temporary increase of testosterone (flare-up phenomenon) followed by downregulation of LHRH receptors. This change in receptor expression leads to a decrease in testosterone down to the castration level within 2 to 4 weeks.

In contrast, *LHRH antagonists* competitively bind LHRH receptors yielding a more rapid decrease in serum testosterone levels [16].

Despite the fact that a vast majority of patients responds well to androgen deprivation therapy (ADT), after two to three years the tumour progresses to a so-called castration-resistant prostate cancer (CRPC) and continues to grow [45]. CRPC is defined as followed [46]:

"Castrate serum testosterone < 50 ng/dL or 1.7 nmol/L plus either

- Biochemical progression: Three consecutive rises in PSA one week apart resulting in two 50% increases over the nadir, and a PSA > 2 ng/mL or,
- Radiological progression: The appearance of new lesions: either two or more new bone lesions on bone scan or a soft tissue lesion using RECIST (Response Evaluation Criteria in Solid Tumours)"

Several studies showed that androgen signalling persists in CRPC despite ADT, thus confirming AR as a promising therapeutic target [47-51]. The mechanisms of AR

activation in CRPC include adrenal gland hormones as alternative androgen source, intratumoural *de-novo* synthesis of androgens, AR overexpression and gain of function mutations [47-51].

Anti-androgens are drugs that directly target the AR. They bind competitively to the AR, thus preventing AR-signalling and inhibiting tumour cell growth. Depending on their chemical structure, these drugs can be divided into steroidal and non-steroidal anti-androgens. Currently, treatment of PCa includes administration of the non-steroidal anti-androgen bicalutamide [16].

For treatment of metastatic castration resistant prostate cancer (mCRPC), however, two new drugs targeting the androgen axis have been developed.

Abiraterone acetate suppresses adrenal and intratumoural testosterone synthesis by inhibiting the enzymatic activity of CYP17 [46].

Enzalutamide, a novel anti-androgen, was approved by the U.S. Food and Drug Administration (FDA) in 2012 for mCRPC treatment in patients resistant to docetaxel to chemotherapy [52]. In addition, in 2014 enzalutamide was also approved for patients without previous chemotherapy [53,54].

In general, enzalutamide targets multiple steps in the androgen receptor signalling pathway. In detail, the anti-androgen binds competitively to the AR and inhibits ligand-induced conformational changes. Besides inhibition of nuclear translocation of the activated AR, enzalutamide also prevents binding of the receptor to the DNA and thus the transcription of androgen-regulated genes (figure 6) [55].
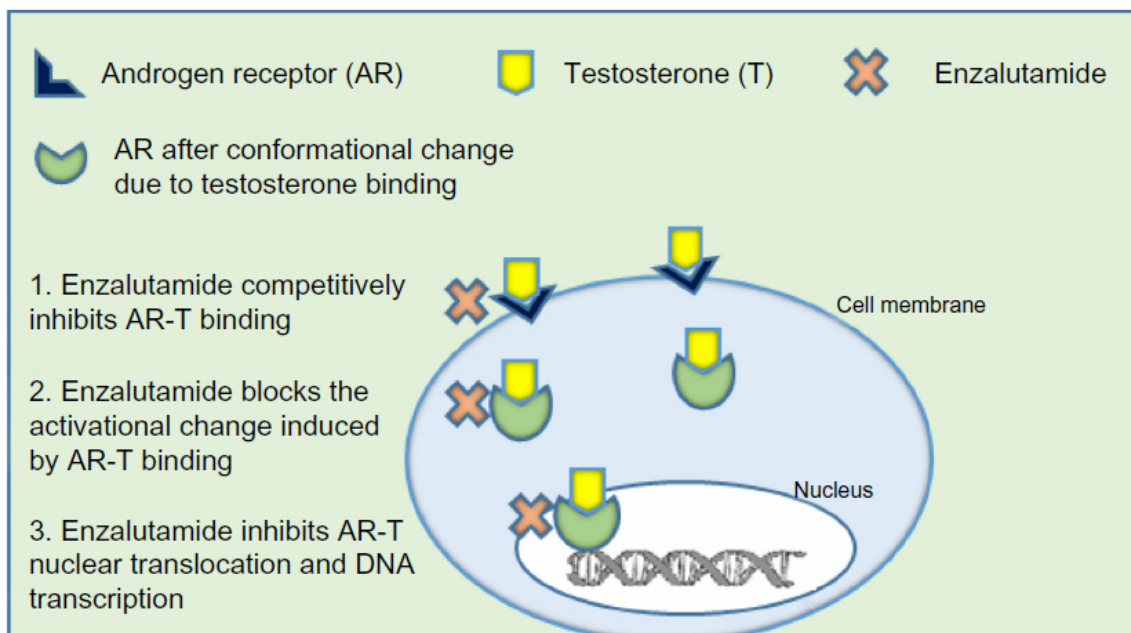
Figure 6: Mechanism of action of androgen receptor inhibiting agent enzalutamide.

Source: [55]

1.2.5.2.2 Chemotherapy

Chemotherapeutic agents such as the FDA-approved drugs docetaxel and cabazitaxel are used to treat symptomatic mCRPC. Docetaxel is also approved for metastatic hormone-naive PCa. Both compounds belong to the taxane family and exert cytotoxic effects on dividing cells, thus predominantly affecting cancer cells. Taxanes bind to, and stabilize microtubules, which causes cell cycle arrest as well as apoptosis [56,57].

1.3 Cullin-RING ligases and the regulatory function of Cand1

1.3.1 The Cullin-RING ligase superfamily

The cullin-RING ligases (CRLs) comprise the largest class of E3 ubiquitin ligases. As part of the ubiquitin-proteasome system, they mediate ubiquitination of protein substrates destined for proteasomal degradation and are, thus, responsible for post-translational regulation of numerous targets [58,59].

CRLs are multi-protein complexes with a common catalytic core consisting of a member of the cullin-family (CUL1-3, 4A, 4B, 5, 7 in human) and a RING (**r**eally **i**nteresting **n**ew **g**ene) protein, also known as HRT1, RBX1 or ROC1 [59,60]. Adaptor proteins, which recruit a variety of different receptors, link specific substrates to the catalytic core, while the RING subunit provides a docking site to the ubiquitin-conjugating enzyme E2 [59].

The archetypical CUL1 CRLs, known as **S**-phase kinase-associated protein 1, **C**UL1, **F**-box proteins (FBPs) (SCF or CRL1), bind substrates via the adaptor protein SKP1 and an FBP which confers substrate specificity (figure 7). This modular composition of CRLs results in a great diversity of the superfamily in terms of function.

In fact, a variety of cellular processes are thought to be regulated by CRLs including DNA replication and cell cycle (reviewed in [59]).
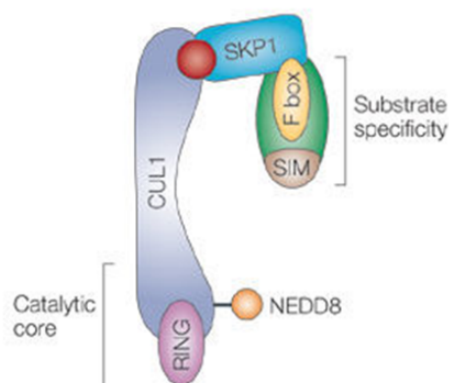
Figure 7: The modular composition of CRLs using the example of SCF.
Source: [59]

1.3.2   Regulation of CRLs by the NEDD8/Cand1 cycle

Besides the regulation of substrate recruitment by the variety of receptor subunits and the required post-translational modifications of the targets, the activity of CRLs is further modulated by the NEDD8/Cand1 cycle. [59,61].

In a process named neddylation, the NEDD8 protein is covalently bound to the CUL-subunit of the enzymatic core by the NEDD8-conjugating enzyme UBC12 resulting in the activation of the CRL. By the intrinsic deneddylating activity of the COP9 signalosome (CSN), NEDD8 is removed, leading to the dissociation of adapter protein and substrate-receptor. Deneddylated cullins are subsequently sequestered by the cullin-associated NEDD8-dissociated protein 1 (Cand1) and held in an inactive state. NEDD8 conjugation again causes the dissociation of Cand1, and thus activation of the ligase (figure 8) [59].
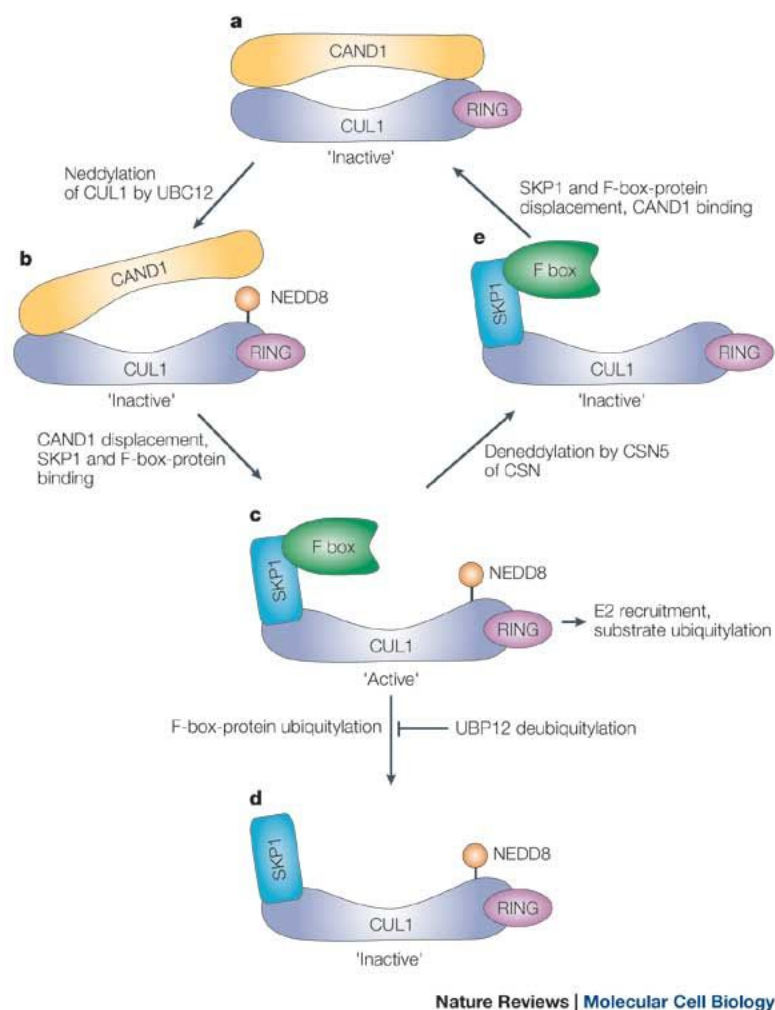
Figure 8: NEDD8/Cand1 cycle dependent regulation of CRL activity.
Source: [59]

It has been previously shown that suppression of Cand1 results in increased CRL activity *in vitro* [62-64]. Other studies, however, showed that Cand1 is required for optimal function of CRLs *in vivo* [64-66]. A potential explanation for this so-called Cand1 paradox was proposed by Schmidt et al. Using a Cand1-homologue deletion strain of *Schizosaccharomyces pombe*, they proved that Cand1 "maintains the cellular balance of CRL1 complexes by preventing rare FBPs from being out-competed for binding to CUL1 by more ample adapters", rather than regulating the stability of FBPs [67]. With these findings, Schmidt et al. assembled a model which explains how CRL complexes undergo continuous auto-ubiquitination in absence of the substrate leading to a destabilization of substrate-receptor subunits. In presence of a substrate, neddylation activates the CRL which then mediates proteasomal degradation of the specific substrate. As soon as the substrate is consumed, CSN catalyses deneddylation and the CRL complex re-enters the Cand1 cycle for maintenance [67].

1.3.3   CRLs and Cand1 in cancer

Aberrant regulation of the ubiquitin system is associated with different pathologies, including the development of cancer [68,69]. Thus, CRLs constituting the largest class of RING finger ubiquitin ligases, are of growing importance in cancer biology and have previously been suggested as attractive targets in tumour therapy [60,70]. Depending on the CRL activity and the bound substrate-receptor, RING-ligases can have both, oncogenic and tumour-suppressive properties. SCF[SKP2] for example, catalyses the ubiquitination of the G1/S cyclin-dependent kinase inhibitor p27, while SCF[FBW7] targets cyclin E or MYC, which are involved in cell proliferation [71]. Deregulation of CRL components such as cullins, CSN subunits or Cand1 has been detected in various tumour entities (table 2) [72].

In non-small cell lung cancer (NSCLC) for example, the mRNA level of Cand1 was found to be increased compared to that in normal tissue [73], whereas in neuroendocrine tumours of the lung the expression was downregulated [74]. Concerning PCa, Cand1 expression was observed to be disrupted in comparison to normal and hyperplastic specimens. In detail, 14.3% of the analysed tumours showed loss of Cand1, whereas in 26.5% an overexpression was detected [75].

Another study, however, showed exclusively lower Cand1 expression in prostatic tumour samples compared to normal tissue [76].

Taken together, disrupted expression levels of Cand1 may be involved in the development and progression of PCa and Cand1 is therefore an interesting target for future studies.

Table 3: Overview of altered Cand1 expression in different tumour entities.

Cand1 downregulation	Cand1 overexpression
Lung cancer, neuroendocrine [74] Prostate cancer [76] Prostate cancer [75]	Lung cancer, NSCLC [73] Prostate cancer [75]

2 Aim of the thesis

Recent evidence supports a correlation between deregulation of the ubiquitin-proteasome system and the development and progression of cancer. In the present study, we, therefore, aimed to elucidate the role of cullin-associated NEDD8-dissociated protein 1 (Cand1), a negative regulator of cullin-RING ubiquitin ligases, in PCa. Thus, we modulated the expression of Cand1 in PCa cell lines and examined the effects on proliferation, cell viability and apoptosis. In this context, we examined not only therapy-naive PCa cells, but included also cell lines resistant to the androgen receptor-inhibiting agent enzalutamide, as we discovered a potential involvement of Cand1 in resistance mechanisms. In order to bridge the gap between our research results and clinical relevance, we also aimed to correlate *cand1* gene expression to overall survival of PCa patients.

3 Material and Methods

3.1 Material

The following tables list all reagents, materials and instruments used in this project.

Human prostate cell lines	Origin	Source
LNCaP	Lymph node metastasis, prostate cancer	American Type Culture Collection (ATCC; Manassas, VA, USA)
PC3	Bone metastasis, prostate cancer	American Type Culture Collection (ATCC; Manassas, VA, USA)
LAPC-4	Lymph node metastasis, prostate cancer	gift from Dr. A. Cato (University of Karlsruhe, Germany)
LNCaP abl	Subline deriving from androgen ablated LNCaP cells	long term cultivation of LNCaP in steroid free medium, source: own [77]
Enzalutamide-resistant LAPC-4	EnzaR subline of LAPC-4	cultivation in presence of increasing concentrations of enzalutamide, source: own [78]
Enzalutamide-resistant LNCaP abl	EnzaR subline of LNCaP abl	cultivation in presence of increasing concentrations of enzalutamide, source: own [78]
DU145	Brain metastasis, prostate cancer	American Type Culture Collection (ATCC; Manassas, VA, USA)
DUCaP	Brain metastasis, prostate cancer	gift from Dr. J Shalken (Radboud University Nijmegen, Netherlands)
NAF, PF179T	hTERT immortalised normal associated fibroblasts (PF 197 primary culture)	gift from Dr. Naomi Goldfinger (Weizmann Institute, Israel)
CAF, PF179T	hTERT immortalised cancer associated fibroblasts (PF 197 primary culture)	gift from Dr. Naomi Goldfinger (Weizmann Institute, Israel)
EP156T	hTERT immortalised prostate epithelial cells	gift from Dr. Naomi Goldfinger (Weizmann Institute, Israel)
RWPE-1	Epithelial cells, benign (immortalised with HPV-18)	gift from Dr. William Watson (University College Dublin, Ireleand)
BPH-1	Benign prostatic hyperplasia epithelial cells (immortalised with SV40 T-antigen)	gift from Dr. J Shalken (Radboud University Nijmegen, Netherlands)

Cell culture	Company	Cat. Nr.
RPMI 1640 without L-glutamine	Lonza	BE12-167F
Fetal Bovine Serum Premium (FBS)	Biowest	S181B-500
Charcoal Stripped Fetal Bovine Serum (CS-FBS)	PAN Biotech	P30-2302
Penicillin/streptomycin	Lonza	17-602E
GlutaMAX-I (100X)	Gibco	35050-038
Sodium pyruvate, 100 mM	Lonza	BE13-115E
HEPES, 1M pH 7.2 sterile filtered	Sigma	H4034-500G
D-(+)-glucose, 250 g/L aqua dest.	Sigma	G7021-1KG
Dulbecco's Phosphate Buffered Saline (DPBS), without Ca^{2+} and Mg^{2+}	LONZA	BE17-512F
Trypsin-Versene (EDTA) Mixture	LONZA	BE17-161E
Enzalutamide (MDV3100)	MedChemExpress	HY-70002
Dihydrotestosterone (DHT)	Sigma Chemical Co.	D5027
MG-132, Z-Leu-Leu-Leu-al	Sigma	C2211
Poly-D-lysine hydrobromide, lyophilized powder, gamma-irradiated	Sigma	P6407
Tissue Culture Flask, T75, Stand., Vent. Cap	Sarstedt	833.911.002
Tissue Culture Flask, T75, Cell+, Vented Cap	Sarstedt	833.911.302
Neubauer-improved, 0.1 mm depth	Marienfeld-Superior	0640010

Transfection	Provider	Cat. Nr.
ON-TARGETplus SMARTpool Human CAND1 siRNA Lot#: 170323; Lot#170530 <u>Target Sequences:</u> GACUUUAGGUUUAUGGCUA (J-015562-09) CGUGCAACAUGUACAACUA (J-015562-10) CAACAAGAACCUACAUACA (J-015562-11) CAUAACAAGCCAUCAUUAA (J-015562-12)	Dharmacon	L-015562-01-0005
ON-TARGETplus Non-targeting Control Pool	Dharmacon	D-001810-10-20
5X siRNA Buffer	Dharmacon	B-002000-UB-100
Lipofectamine® 2000 Transfection Reagent	Invitrogen	11668-019
Cand1 (NM_018448) Human cDNA clone in pCMV6-XL6 cloning vector	OriGene	SC125317
Cloning Vector pCMV6-XL6	OriGene	PCMV6XL6

pCS2-Venus	kindly provided by Christian Ploner, Plastic, Reconstructive & Aesthetic Surgery, Medical University of Innsbruck)	
X-tremeGENE™ HP DNA Transfection Reagent	Roche Diagnostics	6366236001
ViaFect™ Transfection Reagent	Promega	E4982
jetPRIME buffer, sterile filtered 0.2 µm	Polyplus-transfection S.A.	712-60
Corning 50 mL PET Centrifuge Tubes	Corning	430304
JuLI Smart fluorescent cell analyzer	Digital Bio	
Cytation 5 Cell Imaging Multi-Mode Reader	BioTek	
Gen5 Software, Version 3.03	BiotTek	

Plasmid preparation	Company	Cat. Nr.
Lysogeny Broth (LB) Medium: 1% bacto-tryptone 0.5% yeast extract 1% NaCl dissolved in aqua bidest.		
Carbenicillin Disodium Salt BioChemica	AppliChem	A1491
QIAGEN Plasmid Maxi Kit	QIAGEN	12163
QIAGEN-tip 500	QIAGEN	10063
NanoDrop 2000c Spectrophotometer	Thermo Scientific	
NanoDrop 2000/2000c Software; Version 1.4.2	Thermo Scientific	

Restriction digest	Company	Cat. Nr.
1X TAE Buffer: 40 mM Tris 20 mM acetic acid 1 mM EDTA		
1% Agarose Gel: 0.5 g agarose 50 mL 0.5X TAE Buffer		

DNA gel-loading dye (10X):

3.9 mL glycerol

500 µL 10% (w/v) SDS

200 µL 0.5 M EDTA

0.025 g bromophenol blue

0.025 g xylene cyanol

aqua dest. to a final volume of 10 mL

SYBR Safe DNA Gel Stain	Invitrogen	S33102
GeneRuler 1 kb DNA Ladder	Thermo Scientific	SM0311
NcoI, 10 U/µL	Promega	R6513
Buffer D, 10X	Promega	R9921
Bovine Serum Albumin (BSA), acetylated	Promega	R3961
ChemiDoc MP Imaging System	Bio-Rad	

Bradford and BCA assay	**Company**	**Cat. Nr.**
Bradford reagent (5X): 300 mg Coomassie Brilliant Blue G-250 150 mL methanol 150 mL aqua dest. 300 mL 85% phosphoric acid		
Pierce BCA Protein Assay Kit	Thermo Scientific	23227
Spectrophotometer U-2000	Hitachi	
Chameleon V Multitechnology Plate Reader	Hidex	

Western blot analysis		
Cell lysis and SDS-PAGE	**Company**	**Cat. Nr.**
RIPA buffer: 1% Triton X-100 0.5% sodium deoxycholate 150 mM sodium chloride 50 mM Tris-HCl pH 8.0 0.1% sodium dodecyl sulfate (SDS)		

Lysis Buffer: RIPA buffer without SDS (if not stated otherwise) 1% sodium fluoride (NaF),500 mM in aqua dest. 1% PMSF,100 mM in EtOH 1% Triton X-100 1% Phosphatase Inhibitor Cocktail 2 0.5% Protease Inhibitor Cocktail Set III	Sigma Calbiochem	P5726 539134
LDS Sample Buffer (4X) pH 8.5, without dyes: 106 mM Tris-HCl 141 mM Tris base 2% LDS 10% glycerol 0.51 mM EDTA		
Bromophenol Blue	Sigma-Aldrich	114391
NuPAGE Sample Reducing Agent (10X)	Invitrogen	NP0009
NuPAGE LDS Sample Buffer (4X)	Invitrogen	NP0007
Odyssey Protein Molecular Weight Marker, (10-250 kDa)	LI-COR	928-40000
NuPAGE MOPS SDS Running Buffer (20X)	Invitrogen	NP0001
NuPAGE 4-12% Bis-Tris Gel, 1.5mm X 10 well	Invitrogen	NP0335BOX
NuPAGE 4-12% Bis-Tris Gel, 1.0mm X 12 well	Invitrogen	NP0322BOX
XCell SureLock Mini-Cell Electrophoresis System	Invitrogen	EI0002
Western blot	**Company**	**Cat. Nr.**
Amersham Protran, 0.2 μm Nitrocellulose Blotting Membrane	GE Healthcare	10600001
Cellulose Chromatography Paper, Grade 3MM Chr	GE Healthcare	3030-662
NuPAGE Transfer Buffer (20X)	Invitrogen	NP0006
XCell II Blot Module	Invitrogen	EI0002
StartingBlock (TBS) Blocking Buffer	Thermo Scientific	37542
Cand1 (D1F2) Rabbit mAb Ref: 02/2017 Lot# 1; Ref: 02/2017 Lot# 1	Cell Signaling Technology	8759S
Anti-GAPDH Antibody, clone 6C5 Lot#: 2653144	Chemicon	MAB374
Anti-PARP p85 Fragment pAb Lot#: 0000056644	Promega	G7341
IRDye 680RD Goat anti-Mouse IgG (H+L) Lot#: C50721-05	LI-COR	926-68070
IRDye 680RD Goat anti-Rabbit IgG (H+L) Lot#: C60920-06	LI-COR	926-68071

Sonifier 250	Branson	
Odyssey CLx Imaging System	LI-COR	
Image Studio Software, Version 5.2.5	LI-COR	

Caspase, viability and proliferation assays	Company	Cat. Nr.
Caspase-Glo 3/7 Assay Kit	Promega	G8091
96-well Flat Clear Bottom Black Microplates	Corning	3603
Cell Proliferation Reagent WST-1	Roche	11644807001
Thymidine, [methyl-^{3}H]-, 2 Ci/mmol	Hanke Laboratory Products	MT 6034
UniFilter-96 GF/C	PerkinElmer	6005174
MicroScint-20	PerkinElmer	6013621
Harvester 96, Mach III M	Tomtec	
Chameleon V Multitechnology Plate Reader	Hidex	

Immunofluorescence	Company	Cat. Nr.
Fixation Solution: phosphate buffered saline (PBS) 4% paraformaldehyde (PFA)		
Blocking Solution: phosphate buffered saline (PBS) 1% BSA		
Permeabilisation Solution: phosphate buffered saline (PBS) 1% BSA 0.2% Triton X-100		
Cand1 (D1F2) Rabbit mAb Ref: 02/2017 Lot# 1; Ref: 04/2017 Lot# 1	Cell Signaling Technology	8759S
Anti-KRTB antibody, produced in chicken Lot#: SLBC8660V	Sigma	GW22752
Rabbit (DA1E) mAb IgG XP Isotype Control Ref: 12/2014 Lot#19	Cell Signaling Technology	3900S
Goat anti-Rabbit IgG (H+L), Alexa Fluor 555 Lot#: 1608466	Invitrogen	A21428
Goat anti-Chicken IgY (H+L), Alexa Fluor 488 Lot#: 41658A	Invitrogen	A11039
VECTASHIELD Antifade Mounting Medium with DAPI	Vector Laboratories	H-1200

Axio Imager.Z2 microscope	Zeiss
TissueFaxs Cell Analysis System, Version 1.2.4.0116	TissueGnostics

3.2 Methods

3.2.1 Cell culture

The human PCa cell lines LNCaP and PC3 were purchased from American Type Culture Collection (ATCC; Manassas, VA, USA), whereas LAPC-4 were a generous gift from Dr. A. Cato (University of Karlsruhe, Germany). The androgen-independent cell subline LNCaP abl was established by Culig et al. by cultivating androgen-sensitive LNCaP cells in steroid free medium for 87 passages [77]. The enzalutamide-resistant cell lines (EnzaR) of LAPC-4 and LNCaP abl used in this project were generated by Julia Hoefer et al. as described before [78].

Table 4: Overview of used PCa cell lines

Cell line	Origin of cells	AR status	Androgen dependence
LNCaP	Lymph node metastasis, PCa	positive	dependent
PC3	Bone metastasis; PCa	negative	independent
LAPC-4	Lymph node metastasis, PCa	positive	dependent
LNCaP abl	Subline deriving from androgen ablated LNCaP cells	positive	independent, adapted to long term androgen ablation
LAPC-4 EnzaR	EnzaR subline of LAPC-4	positive	?
LNCaP abl EnzaR	EnzaR subline of LNCaP abl	positive	independent

LNCaP and PC3 were grown in RPMI 1640 medium without L-glutamine (Lonza) containing 10% fetal bovine serum (FBS; Biowest), 1% penicillin/streptomycin (Lonza) and 1% GlutaMAX (Gibco). LAPC-4 cells were cultivated in the same medium but additionally supplemented with 1 nM dihydrotestosterone (Sigma Chemical Co.).

LNCaP abl were grown in RPMI 1640 without L-glutamine containing 10% charcoal stripped fetal bovine serum (CS-FBS; PAN Biotech), 1% penicillin/streptomycin,

1% GlutaMAX, 1 mM sodium pyruvate (Lonza), 10 mM HEPES and 2.5 g/L D-(+)-glucose.

EnzaR cell lines were treated with the corresponding medium plus 8 µM enzalutamide (MedChemExpress) for LAPC-4 EnzaR and 13 µM enzalutamide for LNCaP abl EnzaR cells. The corresponding amount of ethanol was used for vehicle-treated control cells.

In vitro cultures were maintained in a humidified atmosphere of 5% CO_2 at 37°C. The cells were routinely grown in T-75 tissue culture flasks (Sarstedt), either using standard growth surface for PC3 or using growth surface for sensitive adherent cells for LNCaP, LAPC-4 and LNCaP abl cells, respectively.

When cells reached about 80% confluence, they were washed once with Dulbecco's Phosphate Buffered Saline (DPBS; Lonza) and incubated with Trypsin-Versene (EDTA; Lonza) for 5 – 10 min. The detached cells were collected by gentle centrifugation at 1200 rpm for 5 min and re-suspended in the respective fresh medium in an appropriate split ratio depending on the planed experiments.

3.2.2 Cand1 downregulation

For downregulation of Cand1 in PCa cells, a pool of four targeting siRNAs (Dharmacon) was used:

Target Sequences:

GACUUUAGGUUUAUGGCUA
CGUGCAACAUGUACAACUA
CAACAAGAACCUACAUACA
CAUAACAAGCCAUCAUUAA

A pool of 4 non-targeting siRNAs served as negative control (siCtrl). Both, siCand1 and siCtrl were resuspended in 1X siRNA Buffer (Dharmacon). For Western blot and Caspase 3/7 Glo Assay, depending on the cell line, 7.5×10^4 to 3.0×10^5 cells were seeded on 6-well plates 24 h before transfection to reach 50 to 60% confluence. For LNCaP, LAPC-4 and LNCaP abl, plates were coated with poly-D-lysine (PDL, Sigma) in order to promote attachment of the cells. Using PET centrifuge tubes (Corning), 3 µL/well Lipofectamine® 2000 (Invitrogen) were incubated in 500 µL of serum free medium for 5 min at room temperature.

50 nM siRNA were added and incubated for other 20 min at room temperature. Afterwards, serum free medium was added to the transfection mixture and 1 mL/well was pipetted gently to the cells. After 6 h of incubation at 37°C, medium containing 20% (CS-) FBS was added to reach a final volume of 2 mL/well. After 96 h, cells were harvested by scraping, washed with DPBS, pelleted at 1800 rpm for 5 min at 4°C and finally shock frozen in liquid nitrogen.

For proliferation and viability assays, depending on the cell line, 3000 – 5000 cells were seeded on 96-well plates to about 50% confluence 24 h before transfection. When using LNCaP, LAPC-4 and LNCaP abl cell lines, plates were coated with PDL in order to promote attachment of the cells. The transfection was carried out as described above for cells in 6-well plates. However, considering the smaller surface area, 0.15 µL/well Lipofectamine® 2000 (Invitrogen) and 50 nM siRNA calculated for 50 µL/well were used and after 6 h medium with 20% (CS-) FBS was added to a final volume of 100 µL/well.

3.2.3 Plasmid amplification and preparation

For amplification of pCMV6-XL6-Cand1 and its empty control vector pCMV6-XL6 (both OriGene), chemically competent *Escherichia coli* (*E. coli*) DH5α were transformed with the respective plasmid. Therefore, 40 µL of thawed cells were mixed with 50 ng of dissolved DNA and incubated on ice for 30 min. Afterwards, tubes were heat pulsed in a 42°C water bath for 60 s and again incubated on ice for 2 min. 190 µL of pre-warmed LB medium were added and incubated at 37°C for 1 h with gentle shaking at 225 rpm. In order to be sure to get single colonies, two different concentrations of each transformation mixture were plated onto two pre-warmed LB agar plates containing 100 µg/mL carbenicillin. After overnight incubation at 37°C, a single colony was picked to inoculate a starter culture in 5 mL LB medium with 100 µg/mL carbenicillin. The starter culture was incubated in a 37°C water bath for 8 h with vigorous shaking and used to further inoculate a main culture of 500 mL. For long term storage, transformed bacteria from the main culture were frozen in 15% glycerol.

Plasmid preparation from the bacterial culture was carried out using the QIAGEN-Plasmid Maxi Kit according to the manufacturer's instructions. Briefly, the cells were harvested by centrifugation at 6000 x g and the DNA was extracted by alkaline lysis. While plasmid DNA renatured upon neutralisation of the solution,

genomic DNA, cell debris and proteins precipitated and were removed by filtration using a pleated filter (Ederol). The flow through was then applied to a QIAGEN-tip 500 which binds the DNA. After two washing steps, the DNA was eluted, precipitated with isopropanol and collected by centrifugation at ≥ 15000 x g at 4°C for 30 min. The DNA pellet was washed with 70% ethanol, air-dried and redissolved in Tris-HCl, pH 8.5. Determination of yield was done with NanoDrop 2000c Spectrophotometer (Thermo Fisher Scientific) at 260 nm and the concentration of the stock solution adjusted to 1 µg/µL for ease of use.

3.2.4   Diagnostic restriction digest of amplified plasmids

In order to verify the presence of the insert in the amplified plasmids, a single-enzyme restriction digest was performed. To this end, 0.5 µg DNA were mixed with 5 U NcoI, 1X Buffer D, 0.1 mg/mL BSA and aqua dest. to a final volume of 10 µL and incubated at 37°C for 1 h. The reaction was stopped by adding 1 µL of 10X DNA gel-loading dye. The resulting fragments and the undigested control were ran on a (1%) agarose gel at an electric field of 75 V for approximately 90 min with 0.5X TAE electrophoresis buffer. 1 µg of the GeneRuler 1 kb DNA Ladder (Thermo Scientific) was loaded as a marker. DNA bands stained with SYBR Safe DNA Gel Stain (Invitrogen) were visualised using the ChemiDoc MP Imaging System (Bio-Rad).

3.2.5   Cand1 overexpression

Depending on the corresponding PCa cell line, 1.2×10^5 to 2.0×10^5 cells were seeded on 6-well plates to 50 to 60% confluence 24 h before transfection. For LNCaP, LAPC-4 and LNCaP abl, the plates were coated with PDL in order to promote attachment of the cells.

pCMV6-XL6-Cand1 plasmid was used for overexpression of Cand1 and empty vector pCMV6-XL6 served as control plasmid (Ctrl). In addition, 0.2 – 0.4 µg of pCS2-Venus were co-transfected to monitor and compare the transfection efficiency when using the different protocols. Venus is a mutated variant of the yellow fluorescent protein (YFP) with improved folding capacities and reduced pH sensitivity [79]. Upon excitation of the protein at 515 nm, Venus emits yellow and green light [80].

In order to reach optimal transfection efficiency, three different transfection reagents have been tested:

Using **X-tremeGENE™** (Roche), 1.6 µg pCMV6-XL6-Cand1 and 3-6 µL of transfection reagent were added to 100 µL of serum free medium and incubated for 15 – 20 min at room temperature. The transfection complex was then added dropwise to the cells without removal of growth medium. After 18 h of incubation, the transfection mixture was replaced with fresh medium.

For transfection with **Lipofectamine**® **2000** (Invitrogen), 5 µL Lipofectamine® 2000 (Invitrogen) were incubated in 500 µL of serum free medium for 5 min at room temperature. 1.6 µg pCMV6-XL6-Cand1 were added and incubated for other 20 min at room temperature. Serum free medium was added to the transfection mixture and 1 mL pipetted gently to the cells. After 18 h of incubation, medium containing 20% (CS-) FBS was added to reach a final volume of 2 mL/well.

For transfection with **ViaFect™** (Promega), 1.6 – 4 µg pCMV6-XL6-Cand1 and 10 or 15 µL of transfection reagent were added to 100 µL of jetPRIME buffer (Polyplus-transfection S.A.) and incubated for 20 min at room temperature. The transfection complex was then added dropwise to the cells without removal of growth medium. After 18 h of incubation, the transfection mixture was replaced with fresh medium. The transfection mixture was replaced with fresh medium after 18 h of incubation.

In case cells were treated with MG132 (Z-Leu-Leu-Leu-al; Sigma-Aldrich), 10 µM/well of the proteasome inhibitor were dropwise added 6 h before harvesting.

72 h after transfection, its efficiency was assessed microscopically with the JuLI Smart fluorescent cell analyser (Digital Bio). In addition, the Cytation 5 Cell Imaging Multi-Mode Reader was used to quantify successful transfection of the Venus plasmid. This was performed by scanning a 13 x 13 matrix in each well with an excitation and emission wavelength of 485 nm and 528 nm, respectively. The intensities were expressed as mean relative fluorescence units (RFU) per well.

Finally, the cells were harvested by scraping, washed with DPBS, pelleted at 1800 rpm for 5 min at 4°C and finally shock frozen in liquid nitrogen.

3.2.6   Western blot analysis

3.2.6.1 SDS-PAGE

Total protein was extracted from cells using RIPA lysis buffer without SDS (if not stated otherwise in the results section) containing 5 mM sodium fluoride (NaF), 1 mM phenylmethyl sulfonyl fluoride (PMSF), 1% Triton X-100, 1% Phosphatase Inhibitor Cocktail 2 (Sigma-Aldrich) and 0.5% Protease Inhibitor Cocktail Set III (Calbiochem). Depending on the size of the cell pellets, 20 – 30 µL of lysis buffer were added and the samples were shaken at 4°C for 1 h. Cell debris was then removed by centrifugation at maximum speed at 4°C for 10 min. Afterwards, samples were diluted in lysis buffer and 4X NuPAGE LDS Sample Buffer (Invitrogen) according to the calculated protein concentrations (see Bradford Assay and BCA Assay). In case of sonication, 70 µL of 1.3X LDS sample buffer without dyes were added to the pellets and the cells lysed using the ultrasound sonicator Sonifier 250 (Branson) with a duty cycle of 40-60%, output control 2 and 6 – 10 pulses. Finally, bromophenol blue (10X; Sigma-Aldrich) and NuPAGE Sample Reducing Agent (10X; Invitrogen) were added to the lysate. The diluted samples were heated at 70°C for 10 min, centrifuged at 6000 rpm for 3 min and finally, 40 – 50 µg of protein were loaded onto the gel. As a molecular mass standard, 2 µL of Odyssey Protein Molecular Weight Marker (LI-COR) were used.

Protein separation was carried out by sodium dodecyl sulfate polyacrylamide gel electrophoresis (SDS-PAGE) in an XCell SureLock Mini-Cell Electrophoresis System at 150 V using NuPAGE 4 – 12% Bis-Tris Protein Gels and 1X NuPAGE MOPS Running Buffer (all Invitrogen).

3.2.6.2 Determination of protein concentration

3.2.6.2.1 Bradford assay

The protein concentration was determined using the Bradford assay. Therefore, a standard curve was generated using bovine serum albumin (BSA) with concentrations ranging from 0 to 40 µg/mL. The samples were diluted in PBS dependent on the expected protein concentration and 1 mL of 1X Bradford reagent was added to each cuvette. The absorbance was measured at 595 nm using the Spectrophotometer U 2000 (Hitachi) and the protein concentrations were calculated based on the standard curve.

3.2.6.2.2 BCA protein assay

The protein concentration of sonicated cells and of cells lysed using RIPA with SDS was determined using the Pierce BCA Protein Assay Kit (Thermo Scientific) and following the manufacturer's protocol. Briefly, six protein standards were prepared by 1:2 serial dilutions of BSA ranging from 0.0625 µg/µL to 2 µg/µL and the samples were diluted 1:8 in the same diluent as the standards. 25 µL of each standard and sample replicate were pipetted into a 96-well plate and 200 µL of working reagent (50:1, Reagent A:B) added to each well. After short term shaking and 30 min of incubation at 37°C, the absorbance was read at 562 nm using the Chameleon V Multitechnology Plate Reader (Hidex).

3.2.6.3 Western blot

The proteins separated by SDS-PAGE were transferred onto a 0.2 µm nitrocellulose blotting membrane (Amersham, GE Healthcare) at 35 Volt (V) for approximately 100 min using an XCell II Blot Module and 1X NuPAGE Transfer Buffer diluted in 10% methanol. The blot was washed with 1X Tris buffered saline (TBS) and blocked with StartingBlock (TBS) Blocking Buffer (Thermo Scientific) for 1 h at room temperature to prevent unspecific binding of antibodies. The primary antibodies were diluted in blocking buffer with 0.1% Tween 20 and incubated overnight rotating at 4°C. The following antibodies were used: Cand1 (1:500, Rabbit monoclonal Antibody (RmAb), Cell Signaling Technology), PARP p85 Fragment (1:500, Rabbit polyclonal Antibody (RpAb), Promega) and GAPDH (1:50000, Mouse monoclonal Antibody (MmAb), Chemicon). After incubation with primary antibodies, the membrane was washed four times for 5 min with 1X TBS with 0.05% Tween 20 (TBS-T) and incubated with an infrared fluorescent dye labelled secondary antibody diluted 1:4000 in phosphate buffered saline (PBS) with 0.2% Tween 20 for 1 h at room temperature and protected from light. Corresponding secondary antibodies used for this project were goat anti-rabbit IgG (for Cand1, PARP p85 Fragment) and goat anti-mouse IgG (for GAPDH) (both LI-COR). After incubation with the secondary antibodies for 1 h at 4°C, the blot was washed four times for 5 min with 1X TBS-T and once with TBS. The protein bands were visualised using the Odyssey CLx Imaging System and further quantified using the Image Studio Software (both LI-COR). Quantification of protein levels were normalised to the housekeeping protein GAPDH used as loading

control and expressed as the fold change or the relative percentage to the respective control.

3.2.7 Caspase-Glo 3/7 Assay

Assessment of apoptosis upon downregulation of Cand1 was carried out by examining the activity of caspase 3 and 7 using the Caspase-Glo 3/7 Assay (Promega). Depending on the cell line, 7.5×10^4 to 3.0×10^5 cells were seeded on 6-well plates, transfected with 50 nM siCand1 or siCtrl and harvested after 96 h of incubation. Cell lysis and protein extraction were performed as described above for SDS-PAGE samples. The measurement was carried out in black 96-well plates (Corning) using lysis buffer as blank. 20 µL of PBS and 5 µL of well vortexed sample were incubated with 25 µL of Caspase-Glo 3/7 Substrate (Promega) on a horizontal shaker for 5 min and another 30 min at room temperature in the dark. Luminescence was measured using the Chameleon V Multitechnology Plate Reader and the results (relative light units, RLU) normalised to the inserted amount of protein determined via Bradford assay.

3.2.8 Cell viability assay

Cell viability upon downregulation of Cand1 was assessed using the Cell Proliferation Reagent WST-1 (Roche). Depending on the cell line, 3000 – 5000 cells were grown in five replicates in 96-well plates and transfected the next day as indicated. After 96 h, WST-1 reagent was added 1:10 to the cells in each well and further incubated at 37°C. The absorbance was measured after 2 h at 420 – 480 nm using the Chameleon V Multitechnology Plate Reader.

3.2.9 Proliferation assay

Cell proliferation upon downregulation of Cand1 was determined by the ^{3}H-thymidine incorporation assay. 24 h before transfection with 50 nM siRNA, depending on the cell line, 3000 – 5000 cells were seeded in five replicates onto 96-well plates. 72 h after transfection, 1 µCi of ^{3}H-thymidine was added to each well and the cells were further incubated at 37°C for 24 h. After freezing the plate at -20°C, cell DNA was harvested on 96-well filter plates (PerkinElmer) and 50 µL of scintillation fluid (PerkinElmer) were added. Incorporated radioactivity was quantified using the Chameleon V Multitechnology Plate Reader.

3.2.10 Immunofluorescence

Depending on the cell line, 1.2 x 10^5 to 2.0 x 10^5 cells were grown on sterile glass coverslips in 6-well plates for 24 h and transfected with 50 nM siCtrl, 50 nM siCand1 or 4 µg pCMV6-XL6-Cand1 (using 15 µL/well ViaFect™) as described above. After 72 h of incubation, cells were washed with PBS and fixed in 4% paraformaldehyde (PFA) for 10 min at room temperature. After a second washing procedure, cells were permeabilised with 0.2% Triton X-100 in PBS with 1% BSA for 5 min on ice. Blocking was carried out with 1% BSA in PBS for 30 min at room temperature, exchanging the solution three times. The cells on the coverslips were incubated for 1 h at 37°C in a wet chamber with 20 µL of primary antibody diluted in blocking solution. The following antibodies were used: Cand1 (1:50, RmAb, Cell Signaling Technology), Rabbit IgG Isotype Control (1:250, RmAb, Cell Signaling Technology) and Cytokeratin-8/KRTB (1:100, Chicken polyclonal Antibody (CpAb), Sigma) for isotype control. After incubation, cells were rinsed in PBS four times, dried on a paper towel and probed for 1 h at 37°C in a wet chamber in the dark with 100 µL of respective secondary antibody (goat anti-rabbit IgG (Alexa Fluor 555), goat anti-chicken IgG (Alexa Fluor 488), both Invitrogen) diluted 1:500 in blocking solution. Again, cells were then rinsed four times in PBS and twice in aqua dest., dried on a paper towel and embedded using VECTASHIELD Antifade Mounting Medium containing DAPI (Vector Laboratories), which stains DNA blue. Finally, cells were visualised by fluorescence microscopy using the Axio Imager. Z2 microscope (Zeiss) and the TissueFaxs Cell Analysis System (TissueGnostics).

3.2.11 Survival Analyses in PCa patients

For survival analysis of PCa patients, we interrogated the publicly available BioProfiling platform [81] for a statistically valid correlation between Cand1 expression and overall survival of PCa patients. For this, the GEO dataset with ID GSE16560 comprising 281 patients with localised PCa [82] was analysed and a Kaplan-Meier plot was generated.

3.2.12 Statistical Analyses

Statistical analyses were performed using GraphPad Prism 5.0. All data is shown as mean plus standard error of mean (SEM) from at least three independent experiments. Differences between two independent groups with not normally distributed values were analysed with the non-parametric Mann-Whitney U test. Significances are encoded as follows: *p<0.05; **p<0.01; ***p<0.001.

4 Results

4.1 Cand1 expression in prostate cell lines

In order to define Cand1 protein expression levels in human prostate cells, a cell line screen of various PCa (LNCaP, LNCaP abl, DUCaP, LAPC-4, CAF, PC3, DU145) and non-cancerous cell lines (EP156T, RWPE-1, BPH-1, NAF) was performed using Western blot. Cand1 was detected in all benign and malignant, epithelial and stromal, androgen receptor positive and negative cell lines (figure 9).
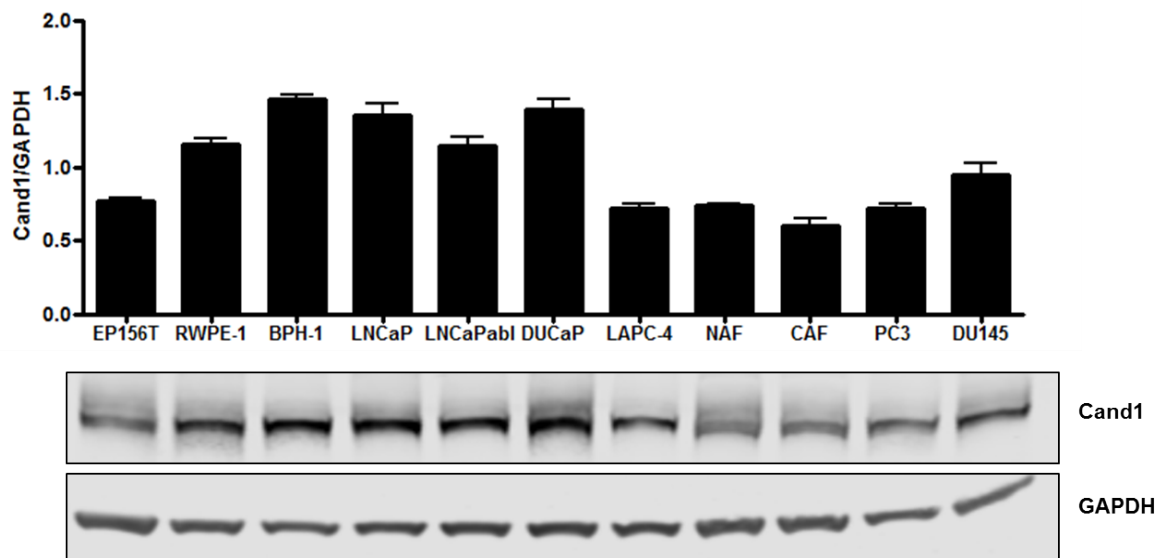
Figure 9: Cand1 expression in human prostate cell lines. Bar chart and representative Western blot images of Cand1 protein expression are shown. The graph displays expression of Cand1 normalised to GAPDH as loading control. Data represent mean + SEM from 3 independent experiments.

4.2 Cand1 in treatment-naive PCa cells

4.2.1 siRNA mediated downregulation of Cand1 in LNCaP and PC3

In order to examine the biological role of Cand1 in PCa cell lines, we modulated its expression in AR positive LNCaP cells as well as in AR negative PC3 cells.

Downregulation of Cand1 was successfully performed using a pool of four specifically targeting small interfering RNAs (siRNAs). A significant decrease of Cand1 on protein level was detected by Western blot analysis after 96 h of incubation using 50 nM siCand1 (figure 10).
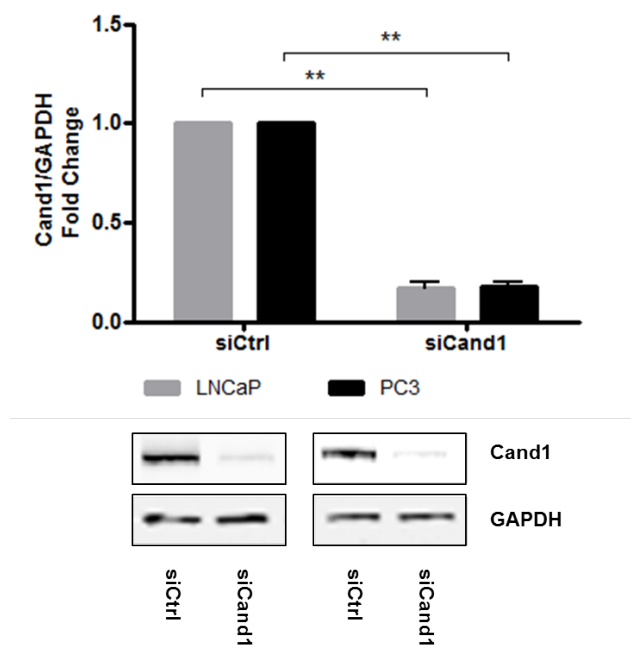
Figure 10: Downregulation of Cand1 in LNCaP and PC3 with specific siRNA. Statistical analyses and representative Western blot images of Cand1 expression are shown. The graph displays fold change of Cand1 expression normalised to GAPDH as loading control. LNCaP and PC3 were transfected with 50 nM siCtrl or siCand1 and incubated for 96 h. Data represent mean + SEM from 6 independent experiments; **: $p < 0.01$.

4.2.2 Functional analyses upon Cand1 knockdown in LNCaP and PC3 cells

4.2.2.1 Cell viability and proliferation assays

Next, we aimed to evaluate the impact of Cand1 downregulation on cell viability and proliferation using WST assay and ^{3}H-thymidine incorporation assay.

Cand1 knockdown significantly reduced the viability of LNCaP cells compared to the control cells (figure 11A). Moreover, a decrease in proliferation by 50% was observed (figure 11B).

In PC3 cells, transfection with siCand1 significantly reduced cell viability and proliferation by 66% and 75%, respectively (figures 11A and B).

Interestingly, AR negative PC3 cells were affected to a greater extent by the downregulation of Cand1 compared to AR positive LNCaP cells (figures 11A and B).

These results suggest an important role of Cand1 in viability and proliferation of PCa cells.
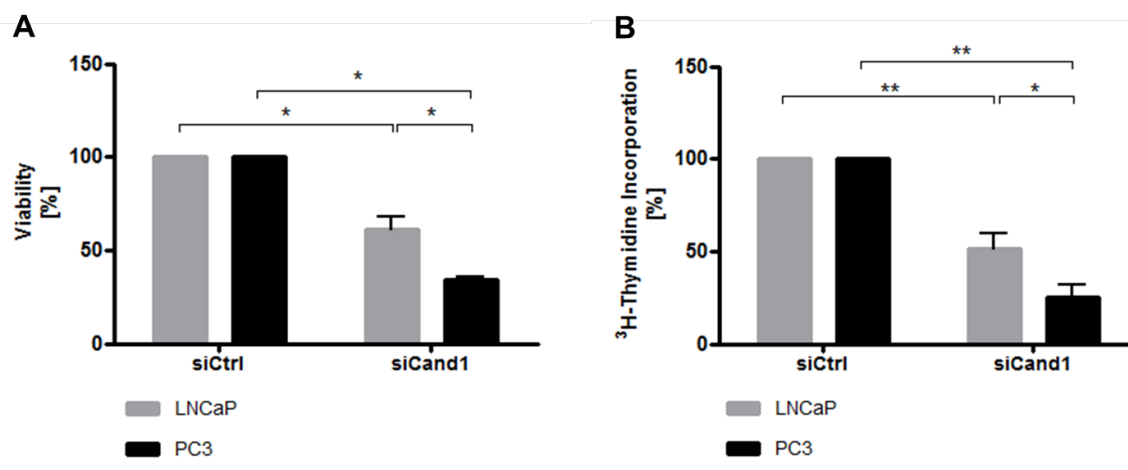
Figure 11: Reduced cell viability and proliferation of siCand1 transfected LNCaP and PC3. Statistical analysis of cell viability (A) and proliferation (B) measured by WST assay and ^{3}H-thymidine incorporation assay, respectively. The graph displays the percentage of viability (A) and proliferation (B) compared to siCtrl. LNCaP and PC3 were transfected with 50 nM siCtrl or siCand1 and incubated for 96 h. Data represent mean + SEM from 4 (A) or 7 (B) independent experiments; *: p<0.05, **: p<0.01.

In addition to cell proliferation and cell viability assay a diminished cellular growth upon downregulation of Cand1 was observed also microscopically. 96 h after

transfection with siCand1, the cell density in the wells was reduced and the amount of dead cells increased compared to the control (figure 12).
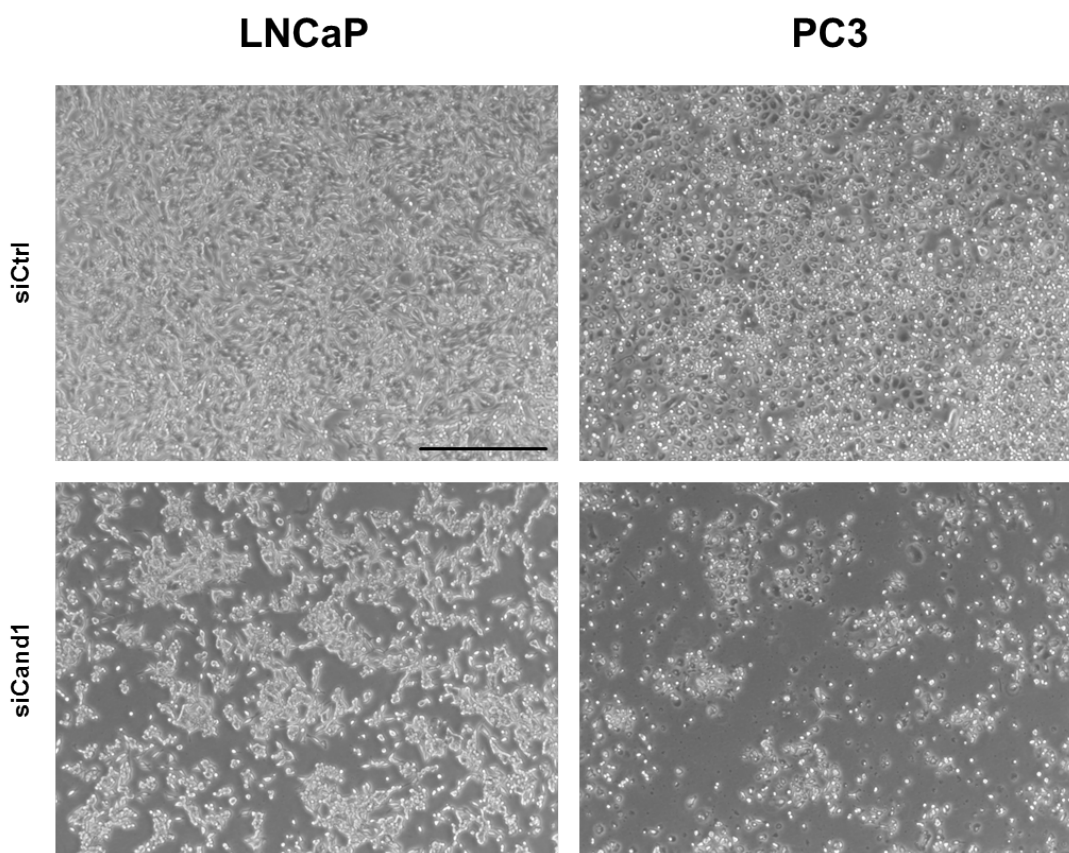

Figure 12: Reduced cell density per well after downregulation of Cand1 in LNCaP and PC3. Representative light microscopic images of LNCaP and PC3 with downregulated Cand1 are shown. Cells were transfected with 50 nM siCtrl or siCand1 and incubated for 96 h. Magnification: 40x. Scale bar: 500 µm.

4.2.2.2 Assessment of apoptotic processes upon Cand1 knockdown

In order to determine whether Cand1 downregulation triggers programmed cell death of human PCa cells, two apoptotic assays, namely determination of cleaved poly (ADP-ribose) polymerase (cPARP) by Western blot as well as measurement of caspase 3/7 activity were performed. Briefly, in response to cell death stimuli, effector caspases – *in vivo* mainly caspase 3 and 7 - are activated and cleave PARP into two fragments. cPARP is an inactive form, thus preventing DNA repair and leading to programmed cell death [83].

4.2.2.2.1 cPARP level

The protein level of cPARP upon Cand1 downregulation was quantified using Western blot analysis.

In LNCaP cells, a significant, 21-fold increase in cPARP level was detected after transfection with siCand1. Also in PC3 cells, this apoptotic marker significantly rose 25.5-fold after transfection.

There were no differences in cPARP level measurable between AR positive LNCaP and AR negative PC3 (figure 13).
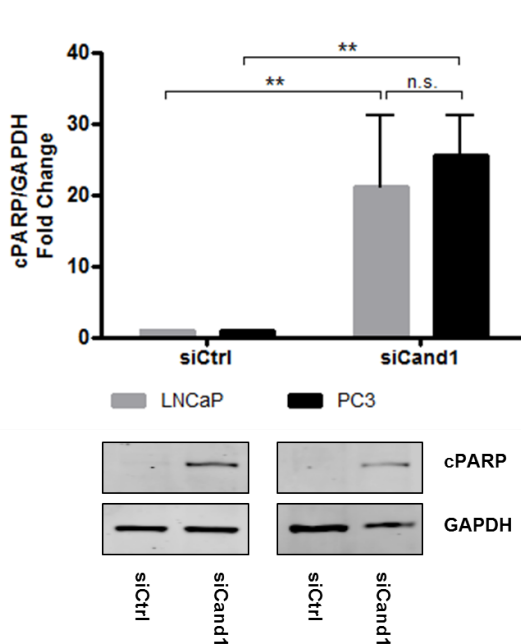

Figure 13: Examination of cPARP level in LNCaP and PC3 after Cand1 downregulation. Statistical analyses and representative Western blot images of cleaved PARP expression are shown. The graph displays fold change of cPARP expression normalised to GAPDH as loading control. LNCaP and PC3 were transfected with 50 nM siCtrl or siCand1 and incubated for 96 h. Data represent mean + SEM from 6 independent experiments, n.s.: not significant, **: $p < 0.01$.

4.2.2.2.2 Caspase 3/7 activity

Activity of caspase 3 and 7 was measured using a luminescent assay. Apoptosis significantly increased in LNCaP and PC3 cells after downregulation of Cand1. Both, AR positive LNCaP and AR negative PC3 showed a comparable increase of the apoptotic marker (figure 14).

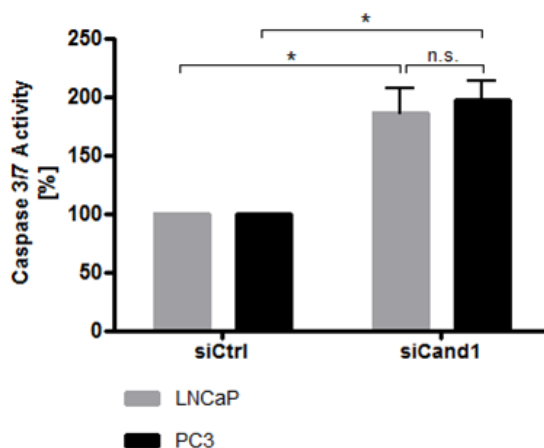Hence, knockdown of Cand1 triggers apoptotic events in human PCa cell lines.

Figure 14: Measurement of caspase 3 and 7 activities in LNCaP and PC3 with downregulated Cand1. Statistical analysis of caspase 3/7 activity is shown. The graph displays the percentage of caspase 3 and 7 activities (RFU) normalised to the amount of protein (µg). Caspase-Glo 3/7 Assay was carried out 96 h after transfection of LNCaP and PC3 with 50 nM siCtrl or siCand1. Data represent mean + SEM from 5 independent experiments; n.s.: not significant, *: $p < 0.05$.

4.2.3 Overexpression of Cand1 in enzalutamide-sensitive PCa cells

After Cand1 downregulation, we next aimed to overexpress Cand1 in LNCaP and PC3 using the overexpression plasmid pCMV6-XL6-Cand1.

4.2.3.1 Diagnostic restriction digest of pCMV6-XL6-Cand1

In order to verify the presence of the gene of interest after amplification of pCMV6-XL6-Cand1 in *E. coli* DH5α, a diagnostic restriction digest was performed. As the definite DNA sequence was routinely not provided by the company, we performed a comparison between the DNA band patterns of the purchased and the amplified plasmid. Therefore, the two plasmids were digested with the restriction enzyme NcoI, which was predicted not to cut the insert, but the vector twice.

The gel electrophoresis of the digested DNA showed three distinct bands for both plasmids, one around 1200 base pairs (bp), and two between 4000 and 6000 bp (figure 15, D). These three fragments are evidence for an additional recognition site for NcoI in the sequences flanking the cloned *cand1* gene.

Also the two uncut plasmids were of comparable size, considering the different diluents (aqua dest. and Tris-HCl) responsible for a dissimilar supercoiling extent and thus for the diverse running behaviour on the gel (figure 15, UD).

Summing up, we could confirm, that the amplified plasmid corresponds to the purchased pCMV6-XL6-Cand1 from OriGene due to the matching DNA band patterns of the two digested plasmids on the gel.
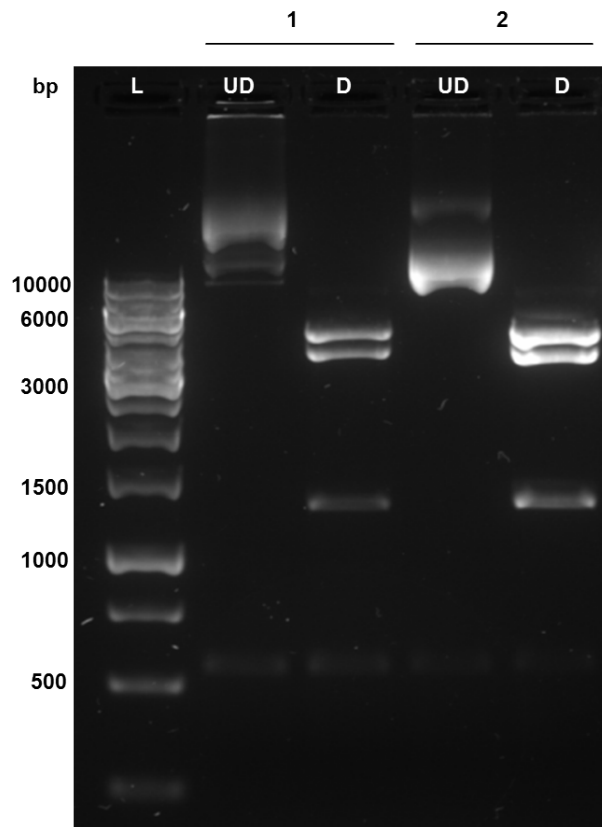

Figure 15: Diagnostic restriction digest of pCMV6-XL6-Cand1. 1% agarose gel electrophoresis of purchased (1) and amplified plasmid (2) pCMV6-XL6-Cand1 is shown. 0.5 µg DNA were digested with 5 U of restriction enzyme NcoI for 1 h at 37°C. (L) denotes 1 kb DNA Ladder (2 µg), (UD) represents undigested and (D) digested samples. (1) purchased plasmid diluted in aqua dest. (2) amplified plasmid diluted in Tris-HCl.

4.2.3.2 Optimisation of transfection efficiency using different transfection reagents

LNCaP cells transfected with 1.6 µg pCMV6-XL6-Cand1 using X-tremeGENE™ as transfection reagent only showed a 1.3-fold increase of Cand1 protein expression after 72 h of incubation (figure 16A). Comparable results were achieved by transfection of PC3. In fact, the merely partial expression of the co-transfected Venus plasmid provided evidence for a low transfection efficiency in both, LNCaP and PC3 (figure 16B). Using fluorescence microscopy we further confirmed the low transfection efficiency by measuring the mean relative fluorescence units (RFU) per area of each well.
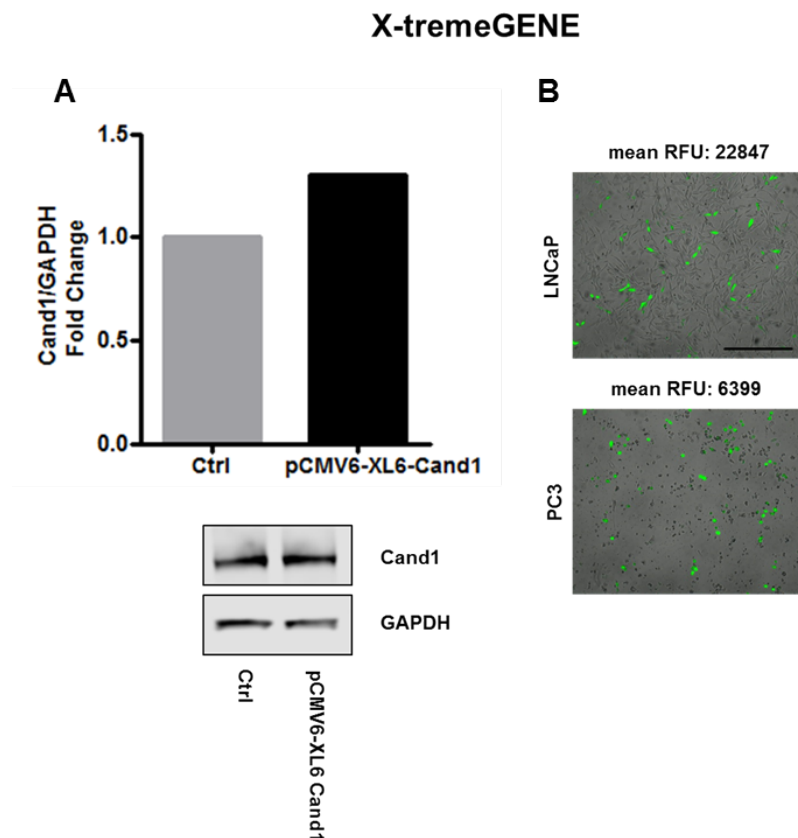
Figure 16: Cand1 overexpression using X-tremeGENE™ as transfection reagent. (A) Bar chart and representative Western blot images of Cand1 expression in LNCaP are shown on the left hand side. The graph displays fold change of Cand1 expression normalised to GAPDH as loading control. (B) The right panel demonstrates transfection efficiency: fluorescence microscopic images of Venus expression in LNCaP and PC3 are shown together with the respective mean RFU. Cells were co-transfected with 1.6 µg pCMV6-XL6-Cand1 and 0.4 µg pCS2-Venus using X-tremeGene™ transfection reagent and incubated for 72 h. n=1.

The minor transfection efficiency demanded optimisation in regard to the transfection reagent used. Thus, we further tested two different transfection reagents, namely Lipofectamine® 2000 and ViaFect™, for introducing pCMV6-XL6-Cand1 into LNCaP and PC3. Comparable cell densities per well were reached when examining the cells for fluorescence after 72 h of incubation (figure 17A). Both cell lines expressed the co-transfected Venus plasmid to a much higher extent when using ViaFect™ as transfection reagent compared to Lipofectamine® 2000 (figure 17B) or X-tremeGENE™ (figure 16B).
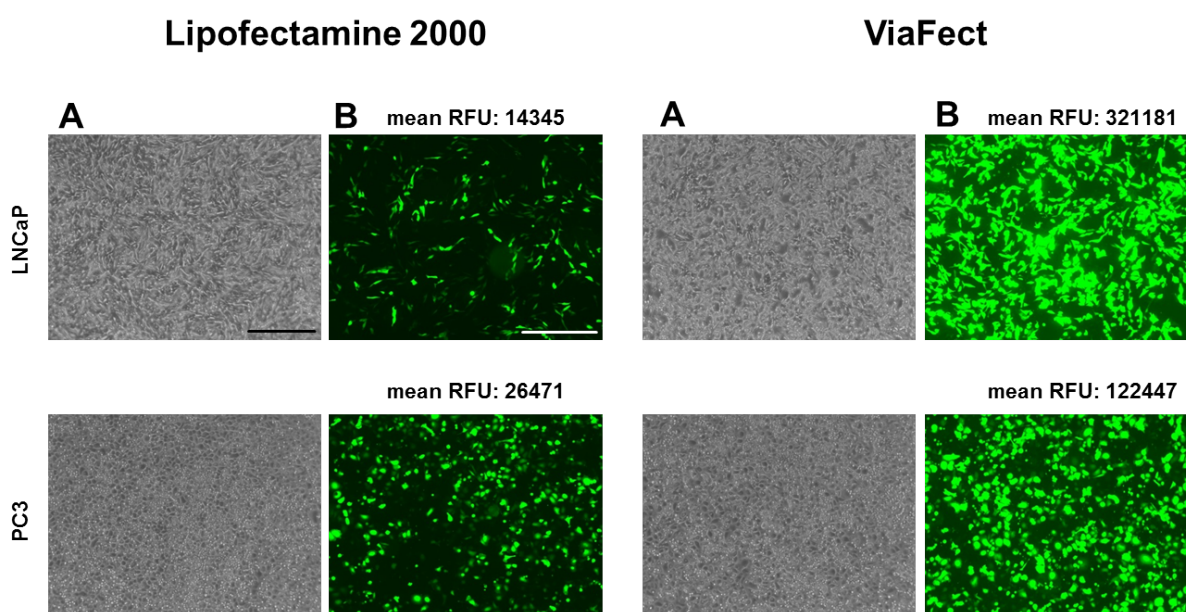
Figure 17: Cell transfection efficiency using Lipofectamine® or ViaFect™ as transfection reagents. Microscopic images of cell density (left panel) and of Venus expression in LNCaP and PC3 are shown together with mean RFU (right panel) for the respective reagent. Cells were co-transfected with 1.6 µg pCMV6-XL6-Cand1 and 0.4 µg pCS-Venus using either X-tremeGENE™, Lipofectamine® 2000 or ViaFect™ as transfection reagents and were incubated for 72 h. n=1.

This difference in transfection efficiency was also reflected by the respective Western blot data. The highest fold change of Cand1 expression in LNCaP was achieved using ViaFect™ (~1.5), followed by X-tremeGENE™ (1.3). The use of Lipofectamine® 2000, however, did not yield in any increase of Cand1 protein expression (figure 18). Comparable results were achieved by transfection of PC3. ViaFect™ was hence selected as suitable transfection reagent for further experiments.

Nonetheless, the degree of Cand1 overexpression was still not satisfactory for performing functional analysis with reliable results. Thus, further optimisations were necessary, which were performed in PC3 cells.
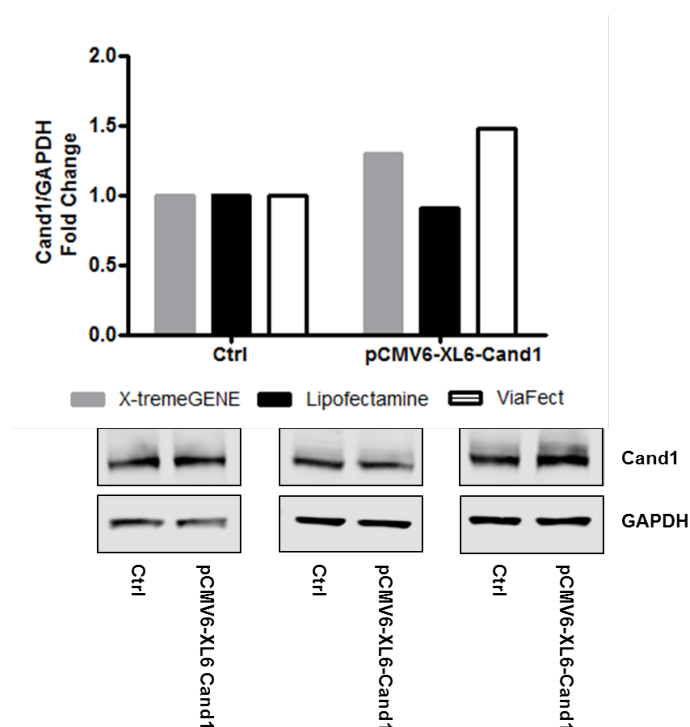

Figure 18: Cand1 overexpression testing different transfection reagents. Bar chart and representative Western blot images of Cand1 expression in LNCaP are shown. The graph displays fold change of Cand1 expression normalised to GAPDH as loading control. Cells were co-transfected with 1.6 µg pCMV6-XL6-Cand1 and 0.4 µg pCS-Venus using either X-tremeGENE™, Lipofectamine® 2000 or ViaFect™ as transfection reagents and were incubated for 72 h. n=1.

For further optimisation of transfection conditions, we tested varying ratios of reagent(µL):DNA(µg). When comparing Cand1 expression after transfection of PC3 using either 10 µL or 15 µL ViaFect™, a higher fold change was achieved using a 15:2 ratio (figure 19A). Given that ViaFect™ only showed low cellular toxicity on PC3 even with higher amounts of reagent, transfections were further performed with 15 µL ViaFect™/well.

Next, we tried to increase the amount of DNA in order to reach a significant Cand1 overexpression. To this end, transfections of PC3 with 2 µg and 4 µg pCMV6-XL6-Cand1 were contrasted. Using 4 µg plasmid resulted in a 2.8-fold

increase of Cand1 expression compared to the respective control and in a 1.5-fold increase compared to transfection using 2 µg DNA (figure 19B).
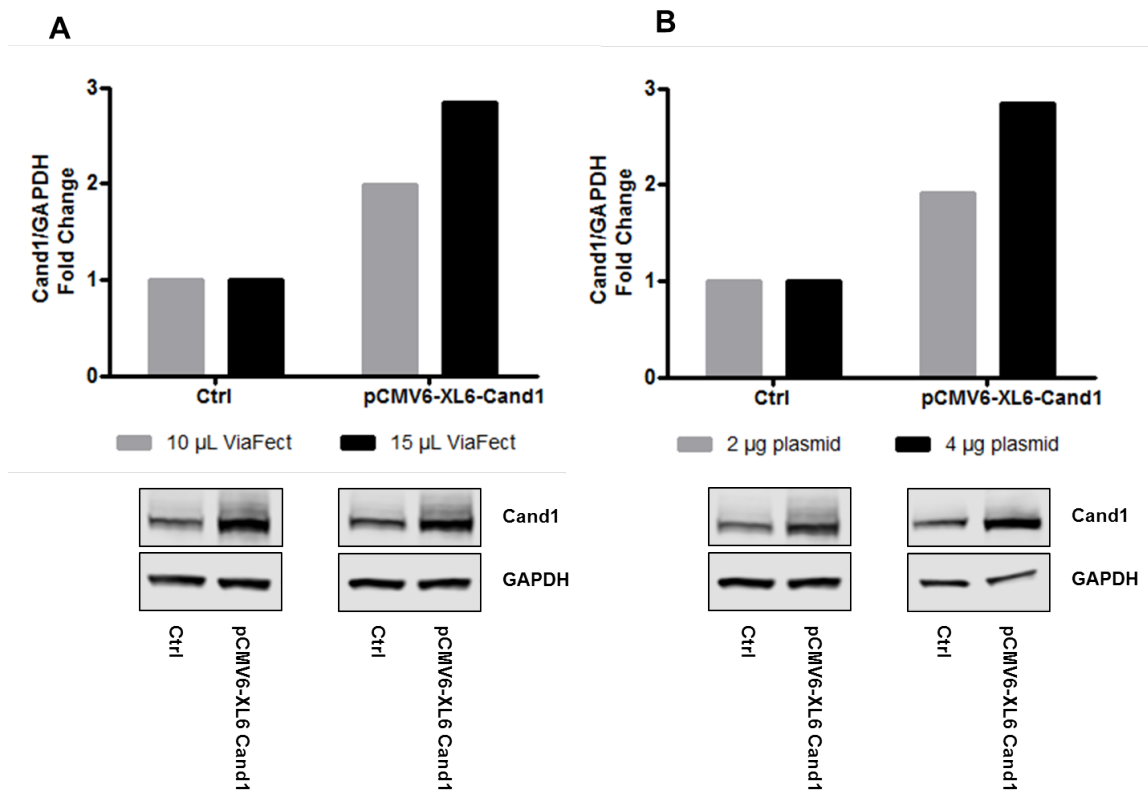

Figure 19: Optimisation of Cand1 overexpression using different reagent:DNA ratios. Bar charts and Western blot images of Cand1 expression in PC3 are shown. The graphs display fold change of Cand1 expression normalised to GAPDH as loading control. Cells were transfected with 2 µg pCMV6-XL6-Cand1 using 10 µL or 15 µL of ViaFect™ (A) or with 2 µg or 4 µg pCMV6-XL6-Cand1 using 15 µL ViaFect™ (B). n=1.

Furthermore, we intended to optimise protein extraction. Therefore, transfected cells were lysed using lysis buffer containing SDS or applying ultrasonic treatment.
Neither the addition of SDS as a denaturing detergent nor physical disruption of cells by sonication significantly improved the outcome (figures 20A and B).
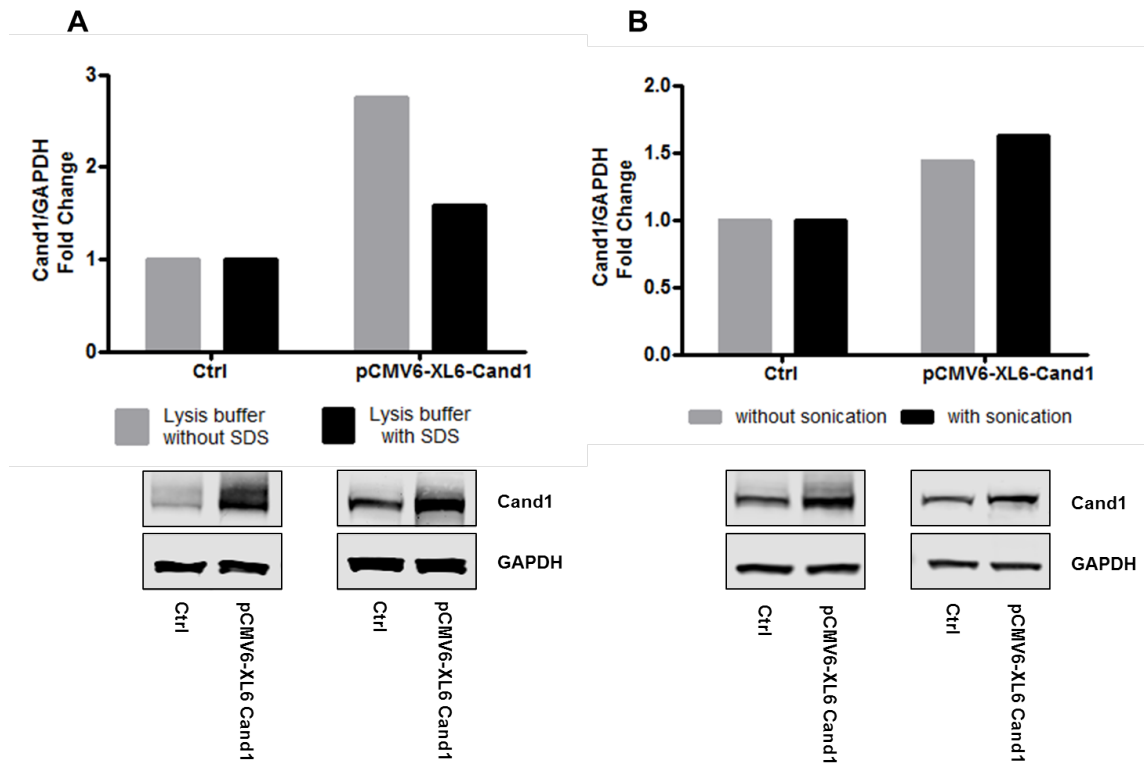
Figure 20: Optimisation of Cand1 protein extraction. Bar charts and Western blot images of Cand1 expression in PC3 are shown. The graphs display fold change of Cand1 expression normalised to GAPDH as loading control. Cells were transfected with 2 µg (A) or 4 µg (B) pCMV6-XL6-Cand1 using 15 µL ViaFect™ and incubated for 72 h. (A) Protein extraction was performed using RIPA lysis buffer with or without SDS. (B) Cell lysis was carried out using solely RIPA lysis buffer or LDS sample buffer (without dyes) combined with sonication. n=1.

4.2.3.3   Examination of a possible regulatory mechanism of Cand1 in PCa cells

We further aimed to uncover a potential regulatory mechanism of Cand1 as a possible reason for the challenges faced in Cand1 overexpression. As Cand1 is involved in the modulation of the activity of CRLs, we speculated a regulation by the ubiquitin-proteasome system. In order to examine a potential negative feedback mechanism of the protein, PC3 transfected with pCMV6-XL6-Cand1 were treated with the proteasomal inhibitor MG132.

The inhibition of degradation of ubiquitinated proteins did not show any difference in Cand1 expression compared to the untreated control (figure 21). However, more biological replicates are needed in order to confirm this preliminary finding.
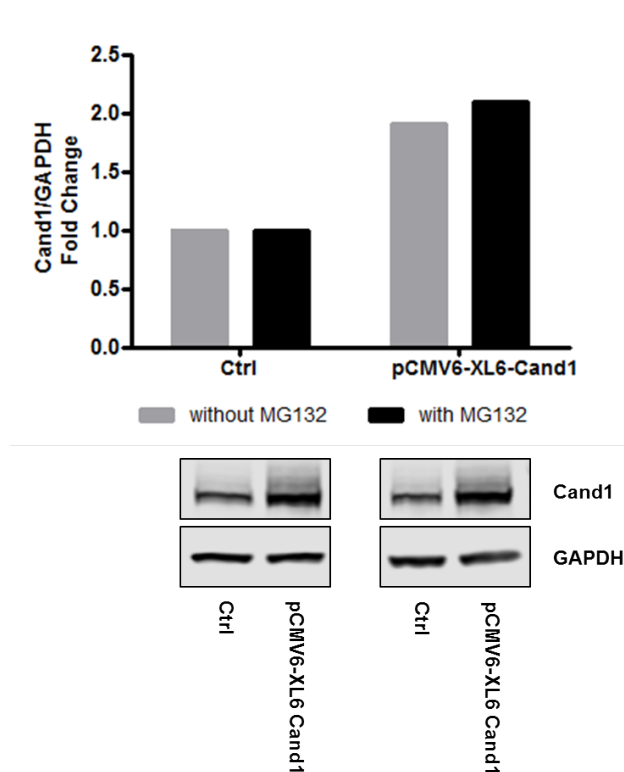
Figure 21: Examination of possible negative feedback regulation of Cand1 by proteasome inhibition with MG132. Bar chart and Western blot images of Cand1 expression in PC3 are shown. The graph displays fold change of Cand1 expression normalised to GAPDH as loading control. Cells were transfected with 2 µg pCMV6-XL6-Cand1 using 15 µL ViaFect™ and incubated for 72 h. 6 h before cell harvesting, 10 µM of proteasome inhibitor MG132 were added. n=1.

After these optimisation steps, we were able to achieve a Cand1 overexpression of maximum 3-fold. Given that we used 4 µg of a commercially available plasmid, the results were not satisfying. Hence, DNA sequencing of the purchased plasmid pCMV6-XL6-Cand1 was performed by Microsynth (Vienna, Austria). This analysis revealed that parts of the vector backbone did not match the sequence data provided by the company. Therefore, a new construction of the Cand1 plasmid was requested. However, the substitute was not received before the end of the master thesis project.

4.2.4 Immunofluorescence staining of Cand1 in LNCaP and PC3

In order to examine and visualize cellular localisation of Cand1, immunofluorescence staining was performed. Thereby, we found Cand1 in both, nucleus and cytoplasm. Moreover, the specificity of the Cand1 antibody for this method could be demonstrated. In both, PC3 and LNCaP cells, Cand1 signal was significantly reduced

after transfection with siCand1. Using the plasmid pCMV6-XL6-Cand1, Cand1 specific staining was increased in a substantial fraction of transfected cells (figure 22 and 23).
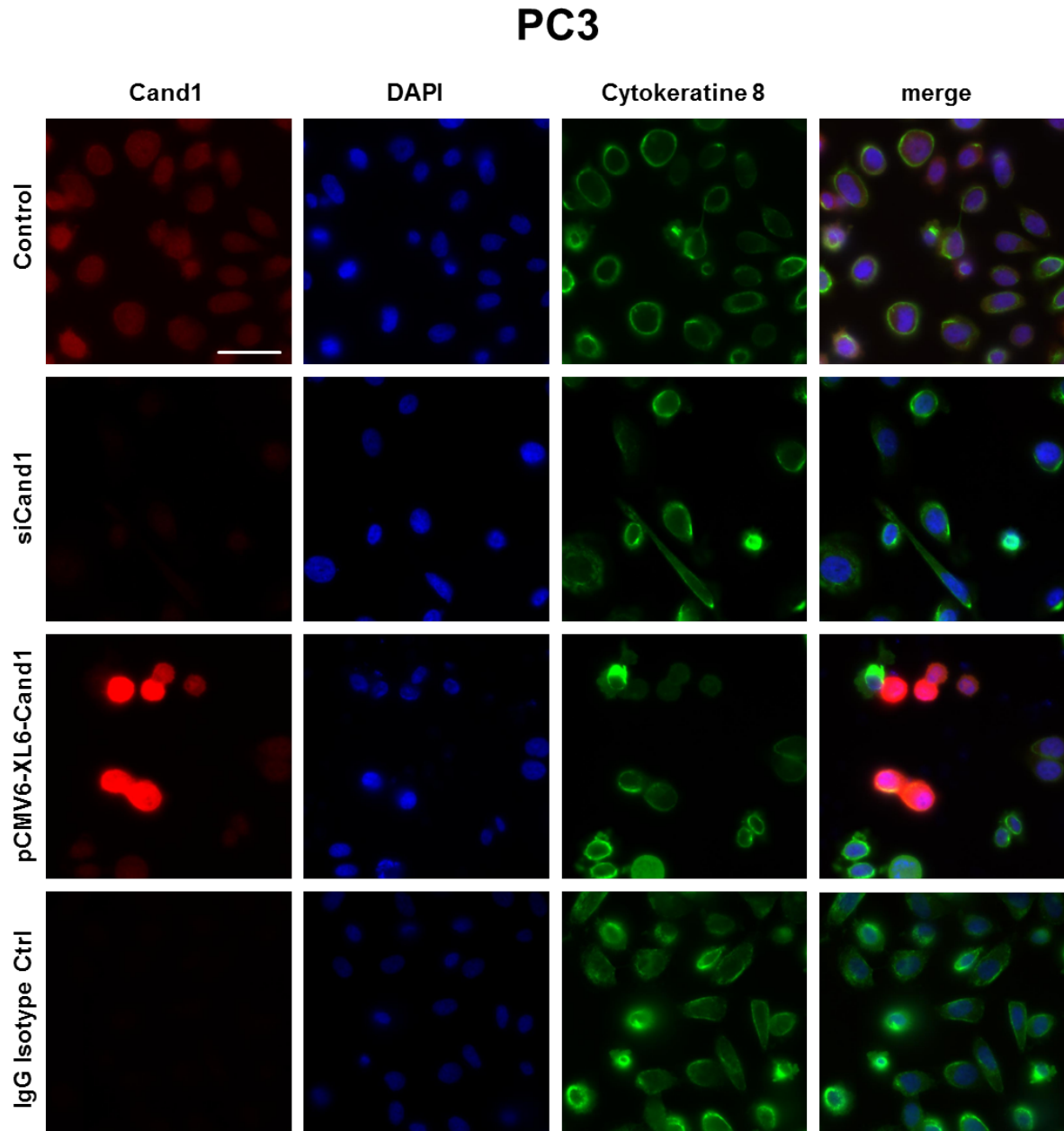
PC3

Figure 22: Immunofluorescence staining of PC3 after downregulation and overexpression of Cand1. PC3 cells were transfected with 50 nM siCtrl (Control), 50 nM siCand1 or 4 µg of pCMV6-XL6-Cand1 and incubated for 72 h. Cand1 was detected using Cand1 RmAb and visualised using goat anti-rabbit secondary antibody (Alexa Fluor 555). Primary antibody anti-KRTB CpAb against Cytokeratin-8 reacted with goat anti-chicken secondary antibody (Alexa Fluor 488). Rabbit mAb IgG served as isotype control. Cell nuclei/DNA were counterstained using DAPI. n=2. Magnification: 400x. Scale bar: 50 µm.
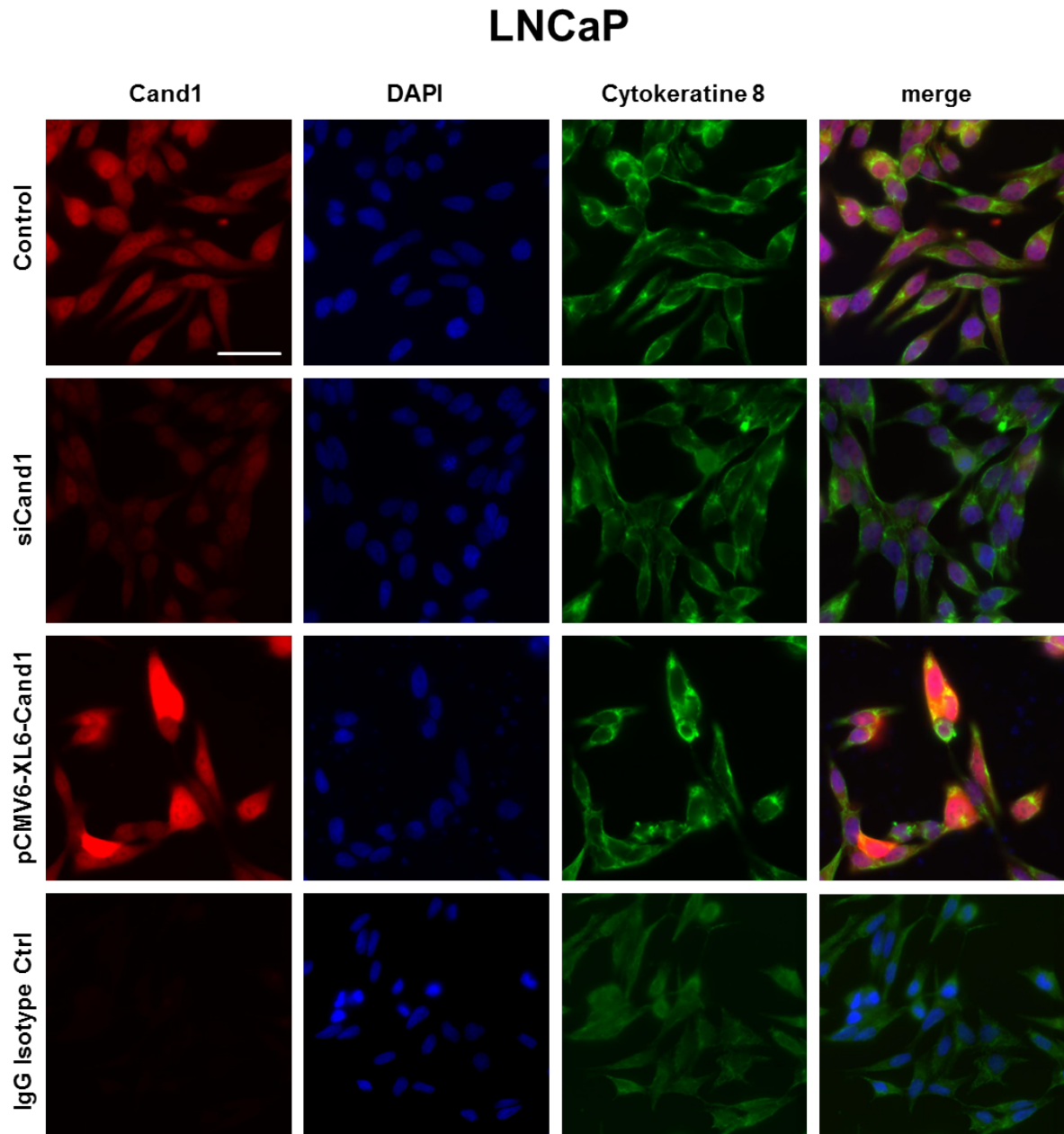
LNCaP

Figure 23: Immunofluorescence staining of LNCaP after downregulation and overexpression of Cand1. LNCaP cells were transfected with 50 nM siCtrl (Control), 50 nM siCand1 or 4 µg of pCMV6-XL6-Cand1 and incubated for 72 h. Cand1 was detected using Cand1 RmAb and visualised using goat anti-rabbit secondary antibody (Alexa Fluor 555). Primary antibody anti-KRTB CpAb against Cytokeratin-8 reacted with goat anti-chicken secondary antibody (Alexa Fluor 488). Rabbit mAb IgG served as isotype control. Cell nuclei/DNA were counterstained using DAPI. n=2. Magnification: 400x. Scale bar: 50 µm.

4.3 Cand1 in enzalutamide-resistant PCa cells

As part of a collaborative project with Bayer Pharma AG, DNA sequencing was performed on EnzaR cells of LAPC-4 and LNCaP abl, sublines established earlier by our research group [78]. In this analysis, Cand1 was found out to be one out of five genes which were mutated in all enzalutamide-treated samples but not in the respective vehicle-treated cells. This finding motivated us to further investigate on the role of Cand1 in EnzaR sublines.

4.3.1 Cand1 downregulation in EnzaR cells of LAPC-4 and LNCaP abl

Successful knockdown of Cand1 in LAPC-4 EnzaR and LNCaP abl EnzaR cells was confirmed using Western blot analysis. Transfection with 50 nM siCand1 resulted in a significant decrease of Cand1 protein expression (figure 24).
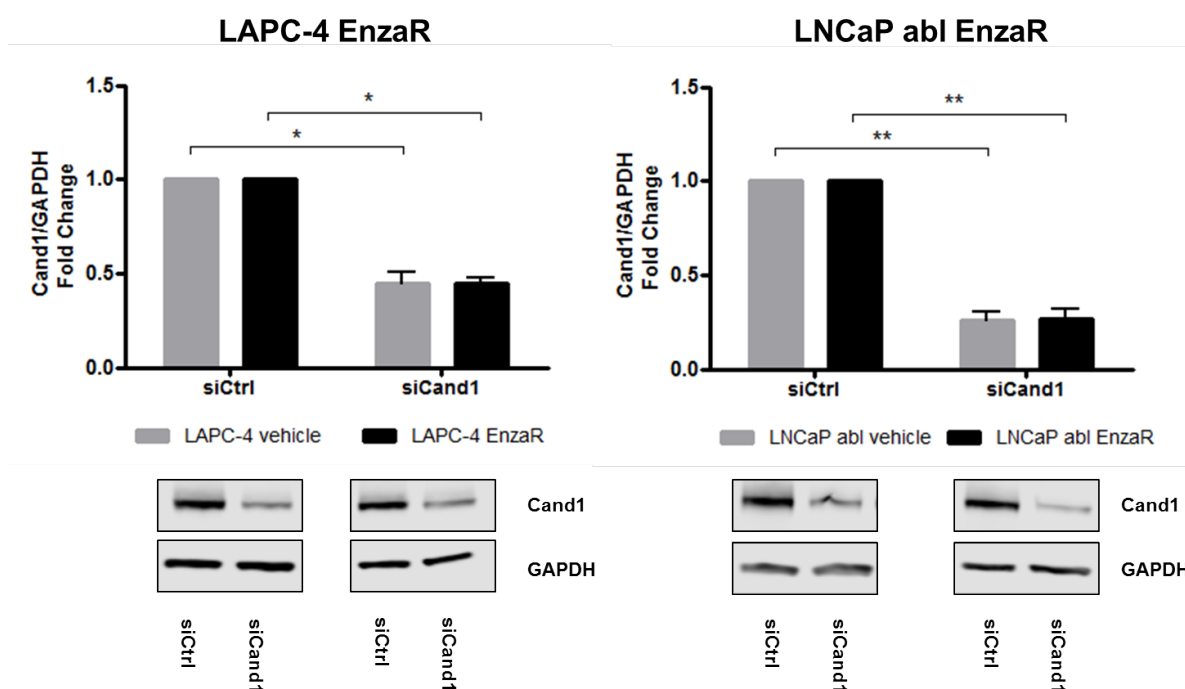

Figure 24: Downregulation of Cand1 in EnzaR cells of LAPC-4 and LNCaP abl with siRNA. Statistical analyses and representative Western blot images of Cand1 expression are shown. The graph displays fold change of Cand1 expression normalised to GAPDH as loading control. All cells were transfected with 50 nM siCtrl or siCand1 and incubated for 96 h. Data represent mean + SEM from 5 (LAPC-4) or 6 (LNCaP abl) independent experiments; n.s.: not significant, *: $p<0.05$, **: $p<0.01$.

4.3.2   Functional analysis upon downregulation of Cand1 in EnzaR cells

4.3.2.1 Viability and proliferation assays

Cell viability and proliferation of EnzaR cells upon downregulation of Cand1 was assessed using WST assay and ^{3}H-thymidine incorporation assay, respectively. Viability of both cell lines was significantly reduced after transfection with siCand1 compared to siCtrl. However, EnzaR cells of LAPC-4 and LNCaP abl were significantly less affected in their viability than the respective control cells (figure 25A).

Both, LAPC-4 EnzaR and vehicle-treated cells were less proliferative after knockdown of Cand1. There was no significant difference observable between the two treatments (figure 25B). In contrast, proliferation of LNCaP abl EnzaR cells was shown not to be inhibited, while vehicle-treated cells displayed reduced ^{3}H-thymidine incorporation (figure 25B). To summarise, Cand1 downregulation has a negative impact on viability of both EnzaR sublines, even though to a different extent, while it only significantly inhibits proliferation of LAPC-4 EnzaR cells.
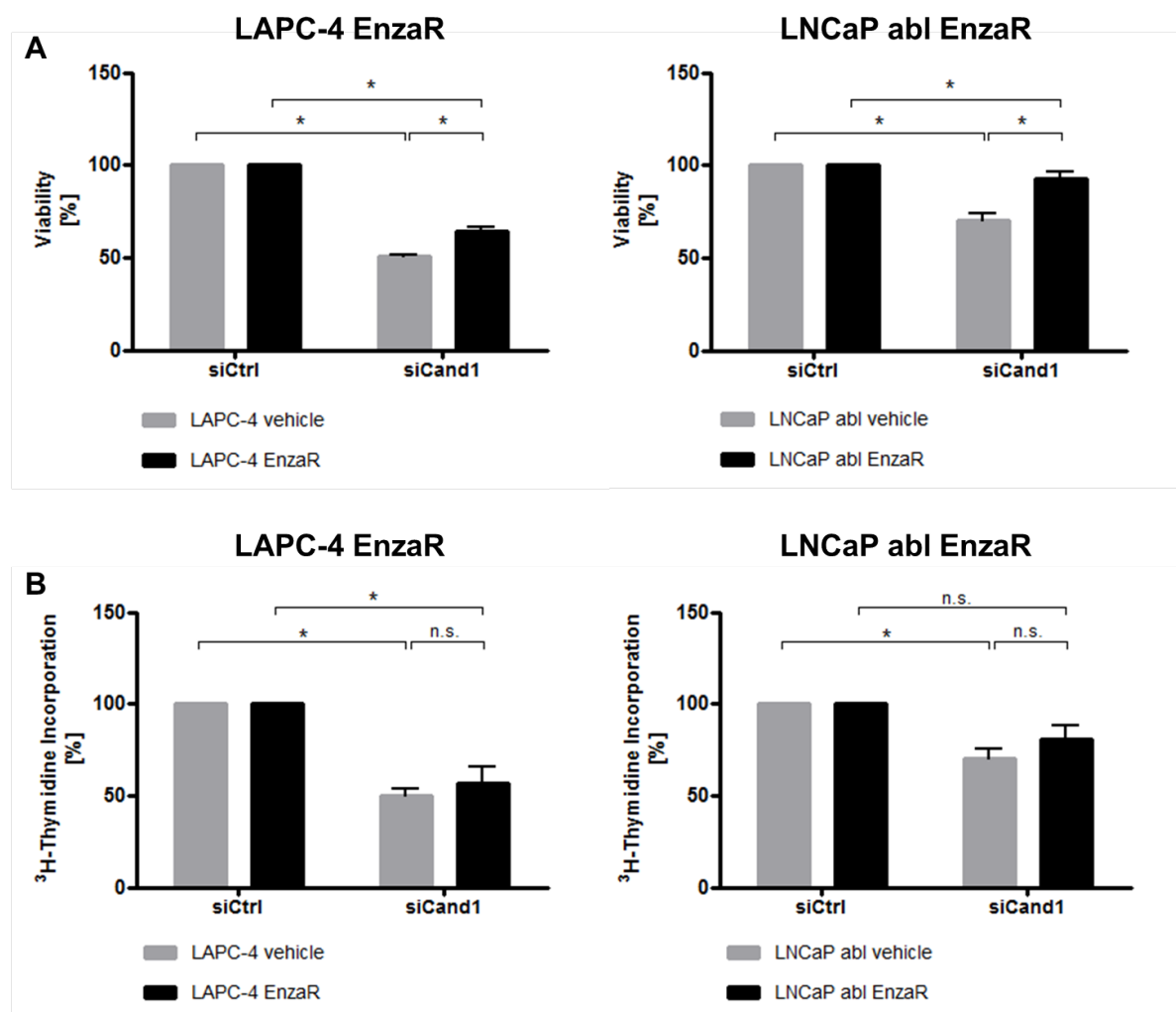
Figure 25: Reduced cell viability and proliferation of siCand1 transfected EnzaR cells of LAPC-4 and LNCaP abl. Statistical analysis of cell viability (A) and proliferation (B) measured by WST assay and ^{3}H-thymidine incorporation assay, respectively. The graphs display the percentage of viability (A) and proliferation (B) compared to siCtrl. All cells were transfected with 50 nM siCtrl or siCand1 and incubated for 96 h. Data represent mean + SEM from 4 independent experiments; n.s.: not significant, *: $p<0.05$.

4.3.2.2   Analysis of apoptosis after Cand1 knockdown in EnzaR cells

4.3.2.2.1 cPARP level

The protein level of cPARP upon Cand1 downregulation was assessed using Western blot analysis.

Vehicle-treated LAPC-4 cells showed a 2.5-fold increase of cleaved PARP after knockdown of Cand1. Also in LAPC-4 EnzaR cells, the cPARP level rose 2.5-fold. Hence, Cand1 downregulation similarly affects apoptosis of EnzaR and treatment-naive LAPC-4 cells (figure 26).

The cPARP level in vehicle-treated LNCaP abl cells did not significantly increase after knockdown of Cand1. Similarly, LNCaP abl EnzaR cells displayed no significant change in cPARP level. Nonetheless, a trend towards an upregulated apoptosis was observed, with EnzaR cells being slightly less affected compared to control cells (figure 26).
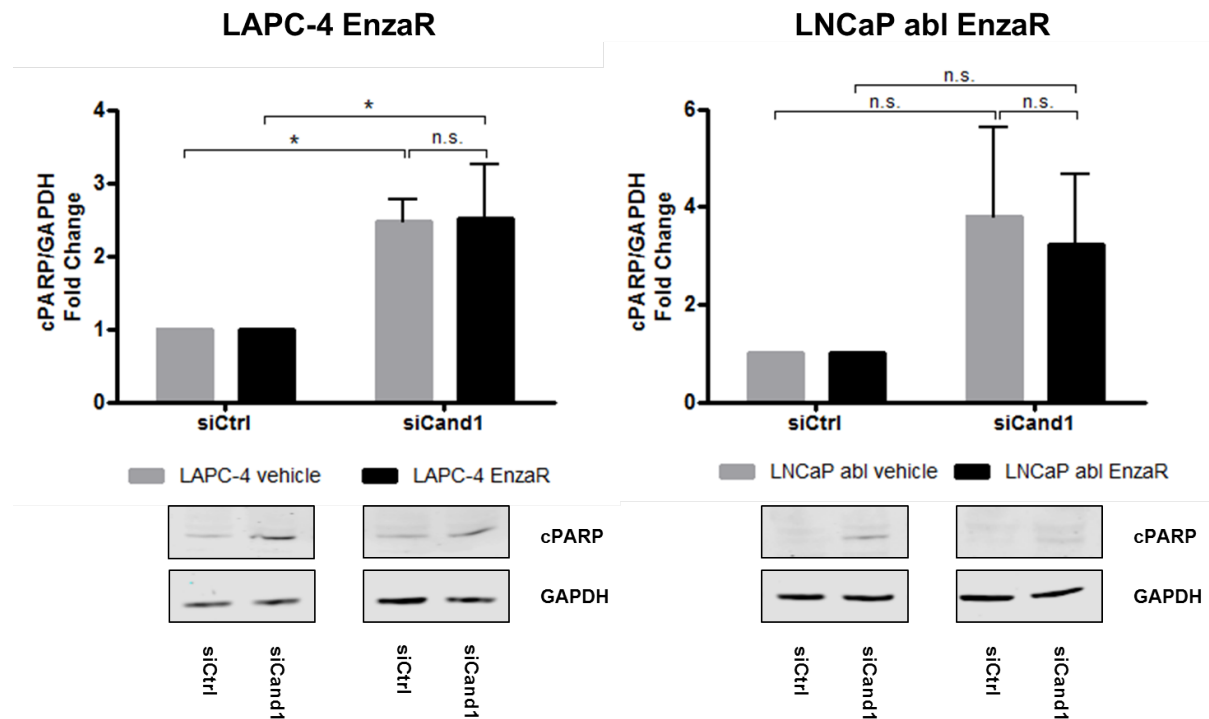

Figure 26: Examination of cPARP level in EnzaR cells of LAPC-4 and LNCaP abl after Cand1 downregulation. Statistical analyses and representative Western blot images of cPARP expression are shown. The graph displays fold change of cPARP expression normalised to GAPDH as loading control. All cells were transfected with 50 nM siCtrl or siCand1 and incubated for 96 h. Data represent mean + SEM from 5 (LAPC-4) or 4 (LNCaP abl) independent experiments; n.s.: not significant, *: p<0.05.

4.3.2.2.2 Caspase 3/7 actvity

Besides cPARP, also caspase 3 and 7 activities were measured as markers for apoptosis.

Analysis of caspase activity of vehicle-treated LAPC-4 cells showed a significant increase of 56% after knockdown of Cand1. In LAPC-4 EnzaR cells, a 20% higher activity of caspase 3 and 7 was measured compared to siCtrl. The difference in apoptosis between vehicle-treated and EnzaR cells was not significant, however, EnzaR cells tended to be less affected by Cand1 knockdown (figure 27).

Downregulation of Cand1 significantly induced apoptosis in vehicle-treated LNCaP abl cells (+45%). EnzaR cells of LNCaP abl showed a 24% increased activity of caspase 3 and 7 after transfection. Hence, Cand1 knockdown triggers apoptosis in both, vehicle-treated and EnzaR LNCaP abl cells, with EnzaR cells tending to be less affected than the control cells (figure 27).
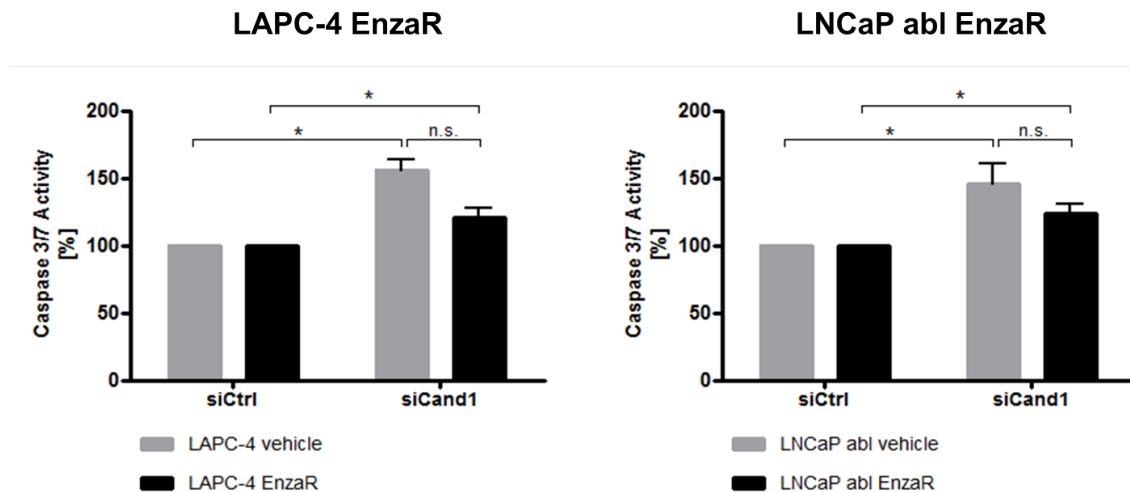

Figure 27: Measurement of caspase 3 and 7 activities in EnzaR cells of LAPC-4 and LNCaP abl with downregulated Cand1. Statistical analysis of caspase 3/7 activity is shown. The graph displays the percentage of caspase 3 and 7 activities (RFU) normalised to the amount of protein (μg). Caspase-Glo 3/7 Assay was carried out 96 h after transfection of the cells with 50 nM siCtrl or siCand1. Data represent mean + SEM from 4 (LAPC-4) or 5 (LNCaP abl) independent experiments; n.s.: not significant, *: $p < 0.05$.

4.4   *Cand1* gene expression-stratified survival analysis of PCa patients

Further, we aimed to validate Cand1 expression in patient samples. Therefore, we interrogated the BioProfiling platform [81] for a statistically valid correlation between Cand1 expression and overall survival of the patient using a GEO dataset (ID GSE16560 [82]) comprising 281 patients with localised PCa.

The resulting Kaplan-Meier plot indicates that low expression of Cand1 is statistically (*p*-value = 0.0144) correlated with an increased overall survival in patients with localised PCa (figure 28).
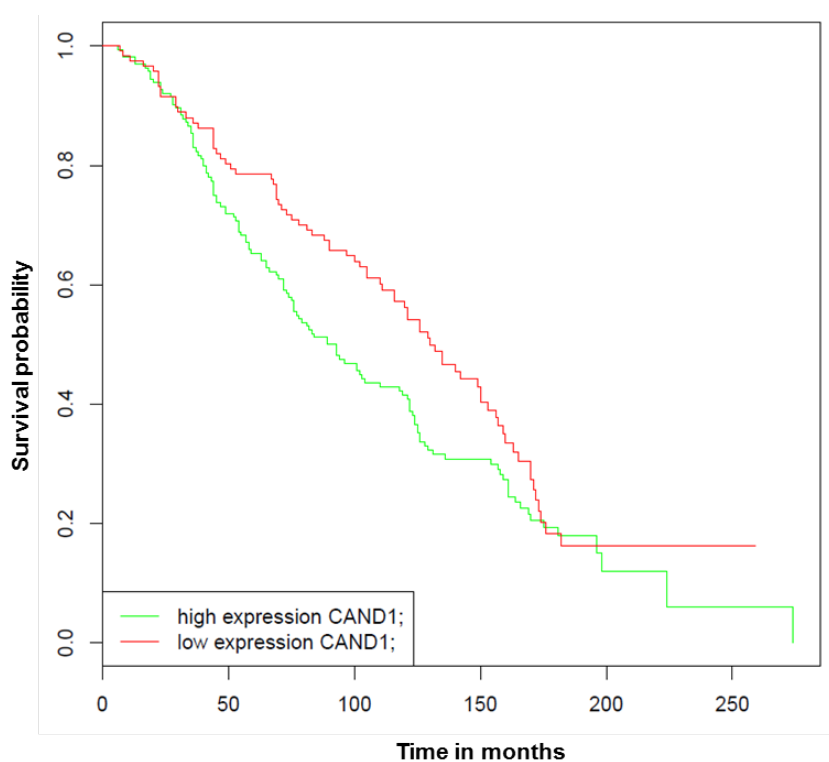
	N	Observed	Expected	(O-E)^2/E	(O-E)^2/V
Group = High Cand1 expression	164	82.2	70.7	1.89	5.99
Group = Low Cand1 expression	117	46.3	57.9	2.31	5.99

Chisq= 6 on 1 degrees of freedom, p= 0.0144
Number of samples: 281

Figure 28: Univariate survival analysis of a PCa patient cohort stratified according to *cand1* expression. The Kaplan-Meier plot represents the probability of overall survival of 281 patients with localised PCa of the GEO dataset ID GSE16560 [82], dichotomised by high or low Cand1 expression. Log-rank test was applied to calculate the *p*-value (1 degree of freedom).

5   Discussion

Despite extensive efforts to discover new therapeutic treatment options for mCRPC, PCa remains one of the leading causes of death among men in Western countries. While early detected, organ-confined PCa can often be cured either by surgery or by primary radiation therapy, up to 50% of patients relapse or already display a locally advanced or metastatic disease stages at the time of diagnosis.

After initial tumour regression in response to androgen deprivation therapy, after a time period of about two years patients experience disease relapse due to the progression to a mCRPC. In the recent years, several new therapeutic options targeting the AR-signalling axis have been developed for this patient population, including the AR-inhibiting agent enzalutamide. Response to these drugs, however, is only temporary, as the majority of treated patients develop drug resistance. Some underlying mechanisms have already been proposed, but research is still ongoing.

In the recent years, the implication of deregulated CRLs in development and progression of various cancer entities has been topic of several research projects. However, the so-called CSN and Cand1 paradoxes, which describe the contradictory results reported from *in vivo* and *in vitro* studies of CRLs, represent a challenging issue. Moreover, due to the fact that CRLs mediate proteasomal degradation of various oncogenic as well as tumour-suppressive proteins, inhibiting CRL activity could result in diverse outcomes. Interestingly, the expression of Cand1, an endogenous key inhibitor of CRL activity, has been shown to be frequently altered in adenocarcinomas of the prostate. In detail, 14.3% of the analysed tumours exhibited a loss of Cand1 expression, whereas 26.5% showed an overexpression [75]. On the other hand, Zhai et al. detected repressed expression of Cand1 in prostate tumour cells compared to the matched normal tissue [76].

Therefore, in the present study we aimed to elucidate the role of Cand1 in PCa by modulating its expression in metastatic PCa cell lines and analysed the resulting functional effects. Briefly, we observed that downregulation of Cand1 caused a significant decrease in cell viability and proliferation in both, AR positive LNCaP and AR negative PC3 cells (see figure 11). These findings contrast the data of Murata et al., showing that Cand1 knockdown promotes proliferation of LNCaP cells [84]. However, according to their published results, Cand1 knockdown in their LNCaP

cells was quite moderate, compromising their conclusions. In contrast, we were able to achieve a significant downregulation of Cand1 in PCa cell lines. This could make the difference in outcome.

Besides impaired cell viability and proliferation, we were able to show that downregulation of Cand1 resulted in a significantly increased apoptosis reflected by increased caspase 3/7 activity and elevated levels of cPARP in LNCaP and PC3 cells (see figures 13 and 14). Consistent with this finding, Rulina et al. demonstrated that Cand1 knockdown induces apoptosis in PCa cell lines [85].

Chua et al. hypothesised that Cand1 differentially regulates CRLs depending on their cellular localisation, as they found Cand1 in human embryonic kidney cells 293 (HEK293) to be predominantly present in the cytoplasm [86]. Here, we provide evidence using immunofluorescence staining that Cand1 is localised in both, nucleoplasm and cytosol of LNCaP and PC3 cells (see figures 22 and 23). Moreover, our finding is supported by validated data from the Human Protein Atlas [87].

DNA sequencing performed on our own generated EnzaR PCa cells revealed *cand1* to be commonly mutated (unpublished data). Therefore, we hypothesised a potential involvement of the protein in the development of drug resistance, and thus extended our research into EnzaR sublines of LAPC-4 and LNCaP abl. Thereby, we could show that Cand1 knockdown negatively affected cell viability and proliferation and induced apoptosis in both, vehicle-treated control cells as well as EnzaR cells (see figures 25-27). Prior to these experiments, we assumed that the knockdown of Cand1 carrying a beneficial mutation would have made EnzaR cells again prone to enzalutamide treatment, thus showing stronger effects upon Cand1 downregulation compared to the therapy-naive control cells. Thus, we conclude that the mutations found in *cand1* of EnzaR cells are not likely to be solely responsible in conferring resistance to the drug. Besides mutations in the AR which result in a gain of function, the synthesis of constitutively active AR splice variants and AR overexpression have been associated with resistance to enzalutamide [88-90], and AR-V7 is used to predict if a patient is likely to respond to enzalutamide therapy [91]. In fact, in a previous study, our research group detected increased expression of a truncated AR variant (AR-V7) as well as gene amplification of the AR in LAPC-4 EnzaR cells.

In contrast, in LNCaP abl EnzaR neither changes in AR copy number nor in the expression of AR-V7 were observed [78], but it was suggested that the glucocorticoid receptor takes over the role of the blocked AR (in press, [92]). Taken together, multiple mechanisms of resistance to the anti-androgen enzalutamide exist and may even co-exist within a cell line or a patient's tumour. Specific genetic alterations of the *cand1* gene, like the mutations found in the EnzaR cells, might contribute to drug resistance as well. This hypothesis, however, needs to be further tested and the impact of these mutations elucidated.

To translate our *in vitro* findings to the *in vivo* patient setting, we determined Cand1 expression in 281 PCa using the BioProfiling platform: Data from 281 patients revealed a correlation between Cand1 levels and overall survival rates of patients with localised PCa. High expression of Cand1 was associated with significantly reduced overall survival of patients compared to low levels of the protein (shown in figure 28). Therefore, we postulate that upregulated expression of Cand1 yields a more aggressive phenotype of the tumour.

To further characterise and understand the observed Cand1 triggered survival disadvantage in PCa patients, we aimed to overexpress Cand1 in the *in vitro* setting in PCa cell lines using the commercially available plasmid pCMV6-XL6-Cand1. As the desired overexpression of Cand1 could not be achieved initially, optimisation of transfection conditions was required. Testing several transfection reagents including Lipofectamine® 2000 and X-tremeGENE™, we found that ViaFect™ is the agent of choice for transfection of the herein tested PCa cell lines with pCMV6-XL6-Cand1. A reagent(µL):DNA(µg) ratio of 15:4 was found to be ideal for efficient transfection. However, only limited success has been achieved in Cand1 overexpression, which could be traced back to the deficiency of the purchased plasmid. This experience highlights the importance of vigorously scrutinizing services, articles and product information provided by companies and other manufacturers.

In the present study we observed individual variations when comparing the available cellular models of PCa. The AR positive LNCaP cell line derived from a lymph node metastasis and is commonly used to represent early stages of PCa due to its androgen-sensitive cell growth. In contrast, the proliferation of bone-metastatic PC3 cells is androgen independent as they do not express the AR [93,94]. Besides androgen sensitivity, however, there are also other marked differences which need to

be considered when comparing these two models. In this study, the high proliferation rate of PC3 cells renders it difficult to conclude whether the significant difference in proliferation between PC3 and LNCaP upon Cand1 knockdown can be attributed to presence or absence of androgen signalling. Phenotypically aggressive cells like PC3 exhibit effects on cell growth to a greater extent than cells with longer doubling times like LNCaP. Therefore, further experiments are needed in order to reveal a possible relation between Cand1 and AR signalling. Interestingly, another study reported androgen-responsive regulation of Cand1 expression in LNCaP cells [84]. However, we did not observe a marked difference in endogenous Cand1 expression between AR positive LNCaP and AR negative PC3 cells.

One of the major problems when utilizing siRNA for protein downregulation is the unpredictability of off-target effects. However, when pooling siRNAs, only low concentrations of each single component are required and, thus, sequence specific off-target effects are diluted below the detection limit. Nevertheless, the pools need to be highly complex in order to achieve elimination of these effects [95]. In this study, we used a pool of four Cand1-targeting siRNAs, the specificity of which was validated beforehand using the Basic Alignment Search Tool (BLAST) from the National Center for Biotechnology Information (NCBI).

In several studies including our own investigation, the induction of apoptosis *in vitro* is analysed by measuring the level of cleaved PARP, as it can easily be detected on Western blot. However, its quantification is technically limited. In our study, this limitation is reflected by a high standard deviation (figures 13 and 26) which is caused by the normalisation of the cPARP signal in siCand1-transfected cells to a signal near the detection limit in siCtrl. In order to overcome the problem of high standard deviation, the signal could be normalised to staurosporine- or etoposide-treated, apoptotic cells [96]. However, we were able to confirm the increase in apoptosis upon Cand1 downregulation using an alternative assay, the luminescent Caspase-Glo 3/7 Assay.

Another alternative approach for detecting apoptosis is fluorescence activated cell sorting (FACS) after staining of cells with FITC-conjugated Annexin V and propidium iodide (PI). This method analyses the percentage of cells with sub-G1 DNA content and which expose phosphatidylserine on their surface. FACS analysis could further be used to assess the impact of different Cand1 expression levels on cell cycle

progression and arrest in various phases. In fact, CRLs target a variety of cell cycle regulatory proteins including p21, p27 and cyclin E, which is why cell cycle analysis would be an interesting topic for future experiments. To summarise this issue, we point out that measuring apoptotic behaviour *in vitro*, more than one method should be used.

When integrating the results obtained in the present study into the model of CRL control proposed by Schmidt et al. [67], Cand1 potentially adopts the role of a time-limiting factor in the two regulatory cycles of Cand1 and CSN. Intracellular availability of Cand1 combined with a deregulated balance or mutation-dependent change in binding affinity of the different substrate-receptors (FBPs in SCF), might influence the faith of a prostatic cell. In fact, overexpression and deletions of FBPs as well as point mutations have been detected in cancer (reviewed in [97]). High Cand1 expression could accelerate the turnover of CRLs, thus, advancing ubiquitination and degradation of tumour suppressor proteins, which are preferentially targeted by the deregulated/mutated FBPs (figure 29). By lowering the level of Cand1, proteasomal degradation would be slowed down resulting in an accumulation of tumour suppressor proteins and induction of apoptosis.
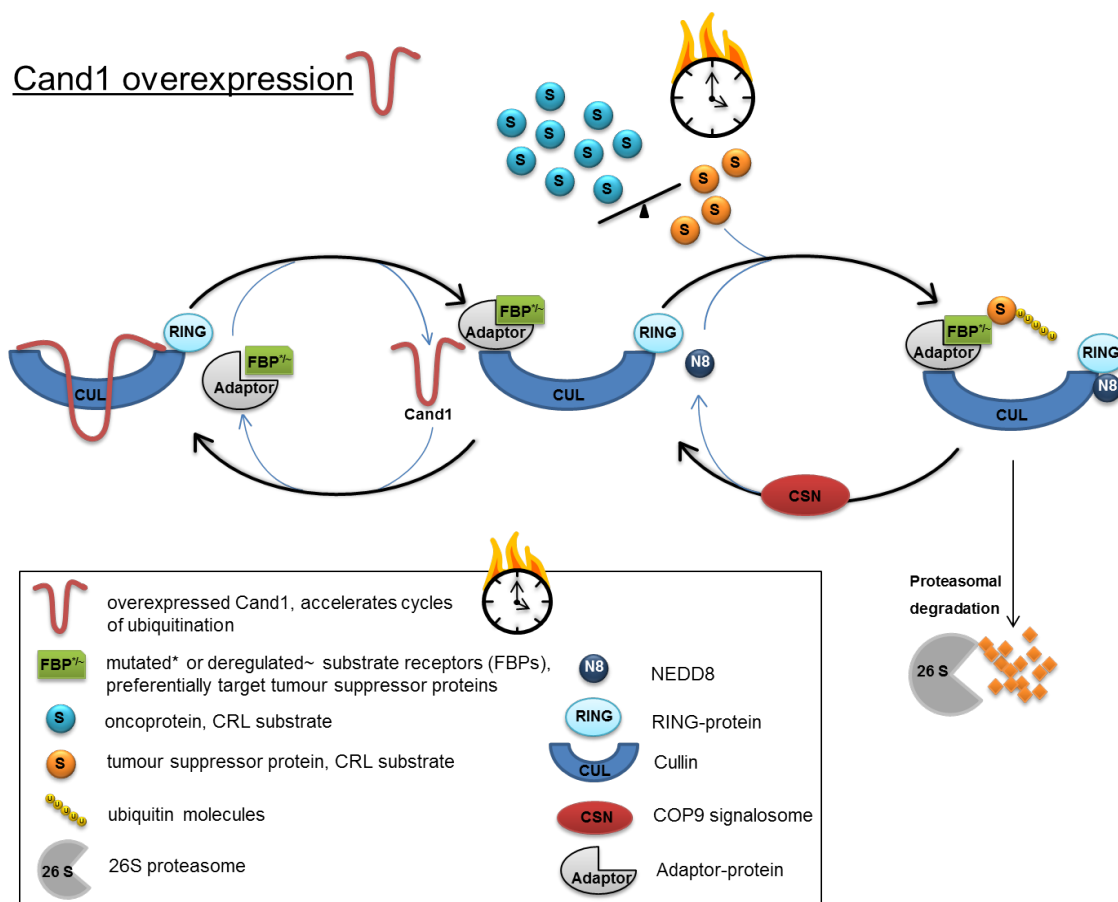
Figure 29: Model for accelerated protein degradation caused by Cand1 overexpression in PCa cells. Overexpression of Cand1 could accelerate the turnover of CRLs and advancing ubiquitination and degradation of tumour suppressor proteins, which are preferentially targeted by deregulated/mutated substrate receptors. Adapted from: [67]

However, in order to clarify the precise regulatory role of Cand1 in PCa, it is also necessary to address the effects of varying Cand1 expression on target proteins and other components of the multi-protein CRL complex with special focus on substrate-receptors. In this regard, Dubiel et al. showed that Cand1 knockdown increases the level of the FBP Skp2 and reduced its substrate p27 in cervical cancer cells (HeLA). Interestingly, the downregulation did not affect the level of FBP Fbxw7 or its target Myc [98]. Therefore, we suggest that downstream effects of varying Cand1 expression are important to be addressed also in PCa cells.

To summarise, our results highlight a significant role of Cand1 in proliferation of PCa cell lines and survival rate of patients with localised PCa. The exact mechanism of function of Cand1 in PCa, however, remains unrevealed. Therefore, we emphasise the importance of further studying the CRL-Cand1 axis in terms of new therapeutic approaches in PCa and of novel predictive biomarkers for treatment-response to enzalutamide.

5.1   Outlook

In this study it has been shown that Cand1 knockdown inhibits the growth of PCa cells *in vitro* by inducing apoptosis. Further experiments will address the impact of a Cand1 overexpression in PCa cell lines with regard to proliferation and apoptosis. Moreover, the effects of differential Cand1 expression on target proteins including p27 and Myc and on other components of the multi-protein CRL complex with special focus on substrate-receptors will be subject of future investigations.

Another topic which needs to be further analysed is the question if *cand1* mutations might confer resistance to enzalutamide treatment. This question will be approached by performing site-directed mutagenesis of the *cand1* gene in order to reveal potential conformational changes of the protein and resulting consequences in binding affinity to other CRL subunits.

For translation into clinics, follow up studies will include immunohistochemical expression analysis of Cand1 in PCa biopsies as well as quantification of Cand1 in serum of enzalutamide-treated patients.

List of abbreviations

ADT	androgen deprivation therapy
Aqua dest.	aqua destillata
AR	androgen receptor
bp	base pair(s)
BPH	benign prostatic hyperplasia
BSA	bovine serum albumin
Cand1	Cullin-associated NEDD8-dissociated protein 1
CmAb	chicken monoclonal antibody
(c)PARP	(cleaved) poly (ADP-ribose) polymerase
cpm	counts per minute
CRL(s)	Cullin-RING ligase(s)
CSN	COP9 signalosome
DAPI	4',6-diamidino-2-phenylindole
DHT	dihydrotestosterone
DPBS	Dulbecco's phosphate-buffered saline
DRE	digital rectal examination
EDTA	ethylenediamine tetraacetic acid
EnzaR	enzalutamide resistant
EtOH	ethanol
FBP(s)	F-box protein(s)
FBS	fetal bovine serum
FDA	United States Food and Drug Administration
GAPDH	glyceraldehyde-3-phosphate dehydrogenase
HEPES	4-(2-hydroxyethyl)-1-piperazineethanesulfonic acid
hTERT	human telomerase reverse transcriptase
IF	immunofluorescence
ISUP	International Society of Urological Pathology
LDS	lithium dodecyl sulfate
LHRH	luteinizing hormone-releasing hormone
(m)CRPC	metastatic castration-resistant prostate cancer
MeOH	methanol
MmAb	mouse monoclonal antibody
NaCl	sodium chloride

NaF	sodium fluoride
PBS	phosphate-buffered saline
PCa	prostate cancer
PFA	paraformaldehyde
PIN	prostatic intraepithelial neoplasia
PSA	prostate-specific antigen
PSMF	phenylmethylsulfonyl fluoride
RCF	relative centrifugal force
RFU	relative fluorescence unit(s)
RING	really interesting new gene
RIPA	radioimmunoprecipitation assay
RmAb	rabbit monoclonal antibody
RpAb	rabbit polyclonal antibody
RPM	revolutions per minute
RPMI	Rosewell Park Memorial Institute
RT	room temperature
SCF	Skp1-Cullin-F-box
SDS	sodium dodecyl sulfate
SDS-PAGE	sodium dodecyl sulfate polyacrylamide gel electrophoresis
SEM	standard error of the mean
CS-FBS	charcoal-stripped FBS
siCand1	Cand1 protein targeting siRNAs (pool of 4)
siCtrl	non-targeting siRNAs, control
siRNA	small interfering ribonucleic acid
TBS	Tris-buffered saline
TBS-T	Tris-buffered saline with Tween20
TNM	tumour-node-metastasis
Tris	tris(hydroxymethyl)aminomethane
WST	water soluble tetrazolium

Figure legend

Table legend

References

1. Menche N (2016) Biologie Anatomie Physiologie: Elsevier.

2. Schmidt RF, Lang F, Heckmann M (2011) Physiologie des Menschen - mit Pathophysiologie: Springer.

3. Benninghoff A, Drenckhahn D (1993) Anatomie: Makroskopische Anatomie, Embryologie und Histologie des Menschen: Urban & Fischer/Elsevier GmbH.

4. King Strasinger S, Schaub Di Lorenzo M (2014) Urinalysis and body fluids: F.A. Davis Company.

5. Plant TM, Zeleznik AJ (2014) Knobil and Neill's Physiology of Reproduction: Academic Press.

6. Verze P, Cai T, Lorenzetti S (2016) The role of the prostate in male fertility, health and disease. Nat Rev Urol 13: 379-386.

7. Walsh PC, Retik A, Darracott Vaughan EJ, Wein AJ (2002) Campbell's Urology: Saunders & Co.

8. Senisi Scott A, Fong E (2016) Body Structures and Functions: Delmar Cengage Learning.

9. Selman SH (2011) The McNeal prostate: a review. Urology 78: 1224-1228.

10. McNeal JE (1981) The zonal anatomy of the prostate. Prostate 2: 35-49.

11. Vargas HA, Akin O, Franiel T, Goldman DA, Udo K, et al. (2012) Normal central zone of the prostate and central zone involvement by prostate cancer: clinical and MR imaging implications. Radiology 262: 894-902.

12. Ferlay J, Soerjomataram I, Dikshit R, Eser S, Mathers C, et al. (2015) Cancer incidence and mortality worldwide: sources, methods and major patterns in GLOBOCAN 2012. Int J Cancer 136: E359-386.

13. Siegel RL, Miller KD, Jemal A (2016) Cancer statistics, 2016. CA Cancer J Clin 66: 7-30.

14. Kheirandish P, Chinegwundoh F (2011) Ethnic differences in prostate cancer. Br J Cancer 105: 481-485.

15. Heidenreich A, Bellmunt J, Bolla M, Joniau S, Mason M, et al. (2011) EAU guidelines on prostate cancer. Part 1: screening, diagnosis, and treatment of clinically localised disease. Eur Urol 59: 61-71.

16. Schmelz HU, Sparwasser C, Weidner W (2014) Facharztwissen Urologie: Differenzierte Diagnostik und Therapie: Springer.

17. Breast Cancer Linkage C (1999) Cancer risks in BRCA2 mutation carriers. J Natl Cancer Inst 91: 1310-1316.

18. Eeles RA, Olama AA, Benlloch S, Saunders EJ, Leongamornlert DA, et al. (2013) Identification of 23 new prostate cancer susceptibility loci using the iCOGS custom genotyping array. Nat Genet 45: 385-391, 391e381-382.

19. Tavtigian SV, Simard J, Teng DH, Abtin V, Baumgard M, et al. (2001) A candidate prostate cancer susceptibility gene at chromosome 17p. Nat Genet 27: 172-180.

20. Castro E, Goh C, Olmos D, Saunders E, Leongamornlert D, et al. (2013) Germline BRCA mutations are associated with higher risk of nodal involvement, distant metastasis, and poor survival outcomes in prostate cancer. J Clin Oncol 31: 1748-1757.

21. Gallagher DJ, Gaudet MM, Pal P, Kirchhoff T, Balistreri L, et al. (2010) Germline BRCA mutations denote a clinicopathologic subset of prostate cancer. Clin Cancer Res 16: 2115-2121.

22. Marcelli M, Ittmann M, Mariani S, Sutherland R, Nigam R, et al. (2000) Androgen receptor mutations in prostate cancer. Cancer Res 60: 944-949.

23. Shi XB, Ma AH, Xia L, Kung HJ, de Vere White RW (2002) Functional analysis of 44 mutant androgen receptors from human prostate cancer. Cancer Res 62: 1496-1502.

24. Ilic D, Misso M (2012) Lycopene for the prevention and treatment of benign prostatic hyperplasia and prostate cancer: a systematic review. Maturitas 72: 269-276.

25. Key TJ (2014) Nutrition, hormones and prostate cancer risk: results from the European prospective investigation into cancer and nutrition. Recent Results Cancer Res 202: 39-46.

26. Leitzmann MF, Rohrmann S (2012) Risk factors for the onset of prostatic cancer: age, location, and behavioral correlates. Clin Epidemiol 4: 1-11.

27. Lippman SM, Klein EA, Goodman PJ, Lucia MS, Thompson IM, et al. (2009) Effect of selenium and vitamin E on risk of prostate cancer and other cancers: the Selenium and Vitamin E Cancer Prevention Trial (SELECT). JAMA 301: 39-51.

28. Nelson WG, De Marzo AM, Isaacs WB (2003) Prostate cancer. N Engl J Med 349: 366-381.

29. Bostwick DG, Cheng L (2014) Urologic Surgical Pathology: Saunders.

30. Shen MM, Abate-Shen C (2010) Molecular genetics of prostate cancer: new prospects for old challenges. Genes Dev 24: 1967-2000.

31. Lanzino M, Sisci D, Morelli C, Garofalo C, Catalano S, et al. (2010) Inhibition of cyclin D1 expression by androgen receptor in breast cancer cells--identification of a novel androgen response element. Nucleic Acids Res 38: 5351-5365.

32. Su F, Correa BR, Luo J, Vencio RZ, Pascal LE, et al. (2013) Gene Expression Profiling Reveals Regulation of ERK Phosphorylation by Androgen-Induced Tumor Suppressor U19/EAF2 in the Mouse Prostate. Cancer Microenviron 6: 247-261.

33. Brooke GN, Bevan CL (2009) The role of androgen receptor mutations in prostate cancer progression. Curr Genomics 10: 18-25.

34. Pienta KJ, Bradley D (2006) Mechanisms underlying the development of androgen-independent prostate cancer. Clin Cancer Res 12: 1665-1671.

35. Lonergan PE, Tindall DJ (2011) Androgen receptor signaling in prostate cancer development and progression. J Carcinog 10: 20.

36. Mattsson JM, Ravela S, Hekim C, Jonsson M, Malm J, et al. (2014) Proteolytic activity of prostate-specific antigen (PSA) towards protein substrates and effect of peptides stimulating PSA activity. PLoS One 9: e107819.

37. Heidegger I, Fritz J, Klocker H, Pichler R, Bektic J, et al. (2015) Age-Adjusted PSA Levels in Prostate Cancer Prediction: Updated Results of the Tyrol Prostate Cancer Early Detection Program. PLoS One 10: e0134134.

38. Gleason DF (1966) Classification of prostatic carcinomas. Cancer Chemother Rep 50: 125-128.

39. Humphrey PA (2004) Gleason grading and prognostic factors in carcinoma of the prostate. Mod Pathol 17: 292-306.

40. Gleason DF, Mellinger GT (1974) Prediction of prognosis for prostatic adenocarcinoma by combined histological grading and clinical staging. J Urol 111: 58-64.

41. Epstein JI, Egevad L, Amin MB, Delahunt B, Srigley JR, et al. (2016) The 2014 International Society of Urological Pathology (ISUP) Consensus Conference on Gleason Grading of Prostatic Carcinoma: Definition of Grading Patterns and Proposal for a New Grading System. Am J Surg Pathol 40: 244-252.

42. Pierorazio PM, Walsh PC, Partin AW, Epstein JI (2013) Prognostic Gleason grade grouping: data based on the modified Gleason scoring system. BJU Int 111: 753-760.

43. Baskar R, Lee KA, Yeo R, Yeoh KW (2012) Cancer and radiation therapy: current advances and future directions. Int J Med Sci 9: 193-199.

44. Huggins C, Hodges CV (2002) Studies on prostatic cancer: I. The effect of castration, of estrogen and of androgen injection on serum phosphatases in metastatic carcinoma of the prostate. 1941. J Urol 168: 9-12.

45. Harris WP, Mostaghel EA, Nelson PS, Montgomery B (2009) Androgen deprivation therapy: progress in understanding mechanisms of resistance and optimizing androgen depletion. Nat Clin Pract Urol 6: 76-85.

46. Mottet N, Bellmunt J, Bolla M, Joniau S, Mason M, et al. (2011) EAU guidelines on prostate cancer. Part II: Treatment of advanced, relapsing, and castration-resistant prostate cancer. Eur Urol 59: 572-583.

47. Chen CD, Welsbie DS, Tran C, Baek SH, Chen R, et al. (2004) Molecular determinants of resistance to antiandrogen therapy. Nat Med 10: 33-39.

48. Scher HI, Sawyers CL (2005) Biology of progressive, castration-resistant prostate cancer: directed therapies targeting the androgen-receptor signaling axis. J Clin Oncol 23: 8253-8261.

49. Sharifi N (2013) Mechanisms of androgen receptor activation in castration-resistant prostate cancer. Endocrinology 154: 4010-4017.

50. Tilley WD, Buchanan G, Hickey TE, Bentel JM (1996) Mutations in the androgen receptor gene are associated with progression of human prostate cancer to androgen independence. Clin Cancer Res 2: 277-285.

51. Visakorpi T, Hyytinen E, Koivisto P, Tanner M, Keinanen R, et al. (1995) In vivo amplification of the androgen receptor gene and progression of human prostate cancer. Nat Genet 9: 401-406.

52. Ning YM, Pierce W, Maher VE, Karuri S, Tang SH, et al. (2013) Enzalutamide for treatment of patients with metastatic castration-resistant prostate cancer who have previously received docetaxel: U.S. Food and Drug Administration drug approval summary. Clin Cancer Res 19: 6067-6073.

53. Beer TM, Armstrong AJ, Rathkopf DE, Loriot Y, Sternberg CN, et al. (2014) Enzalutamide in metastatic prostate cancer before chemotherapy. N Engl J Med 371: 424-433.

54. Scher HI, Fizazi K, Saad F, Taplin ME, Sternberg CN, et al. (2012) Increased survival with enzalutamide in prostate cancer after chemotherapy. N Engl J Med 367: 1187-1197.

55. Patel NK, Finianos A, Whitaker KD, Aragon-Ching JB (2014) Advanced prostate cancer - patient survival and potential impact of enzalutamide and other emerging therapies. Ther Clin Risk Manag 10: 651-664.

56. Montero A, Fossella F, Hortobagyi G, Valero V (2005) Docetaxel for treatment of solid tumours: a systematic review of clinical data. Lancet Oncol 6: 229-239.

57. Seruga B, Tannock IF (2011) Chemotherapy-based treatment for castration-resistant prostate cancer. J Clin Oncol 29: 3686-3694.

58. Cordero-Espinoza L, Hagen T (2013) Regulation of Cullin-RING ubiquitin ligase 1 by Spliceosome-associated protein 130 (SAP130). Biol Open 2: 838-844.

59. Petroski MD, Deshaies RJ (2005) Function and regulation of cullin-RING ubiquitin ligases. Nat Rev Mol Cell Biol 6: 9-20.

60. Zhao Y, Sun Y (2013) Cullin-RING Ligases as attractive anti-cancer targets. Curr Pharm Des 19: 3215-3225.

61. Duda DM, Scott DC, Calabrese MF, Zimmerman ES, Zheng N, et al. (2011) Structural regulation of cullin-RING ubiquitin ligase complexes. Curr Opin Struct Biol 21: 257-264.

62. Liu J, Furukawa M, Matsumoto T, Xiong Y (2002) NEDD8 modification of CUL1 dissociates p120(CAND1), an inhibitor of CUL1-SKP1 binding and SCF ligases. Mol Cell 10: 1511-1518.

63. Oshikawa K, Matsumoto M, Yada M, Kamura T, Hatakeyama S, et al. (2003) Preferential interaction of TIP120A with Cul1 that is not modified by NEDD8 and not associated with Skp1. Biochem Biophys Res Commun 303: 1209-1216.

64. Zheng J, Yang X, Harrell JM, Ryzhikov S, Shim EH, et al. (2002) CAND1 binds to unneddylated CUL1 and regulates the formation of SCF ubiquitin E3 ligase complex. Mol Cell 10: 1519-1526.

65. Chuang HW, Zhang W, Gray WM (2004) Arabidopsis ETA2, an apparent ortholog of the human cullin-interacting protein CAND1, is required for auxin responses mediated by the SCF(TIR1) ubiquitin ligase. Plant Cell 16: 1883-1897.

66. Feng S, Shen Y, Sullivan JA, Rubio V, Xiong Y, et al. (2004) Arabidopsis CAND1, an unmodified CUL1-interacting protein, is involved in multiple developmental

pathways controlled by ubiquitin/proteasome-mediated protein Degradation. Plant Cell 16: 1870-1882.

67. Schmidt MW, McQuary PR, Wee S, Hofmann K, Wolf DA (2009) F-box-directed CRL complex assembly and regulation by the CSN and CAND1. Mol Cell 35: 586-597.

68. Hoeller D, Dikic I (2009) Targeting the ubiquitin system in cancer therapy. Nature 458: 438-444.

69. Hershko A, Ciechanover A (1998) The ubiquitin system. Annu Rev Biochem 67: 425-479.

70. Soucy TA, Dick LR, Smith PG, Milhollen MA, Brownell JE (2010) The NEDD8 Conjugation Pathway and Its Relevance in Cancer Biology and Therapy. Genes Cancer 1: 708-716.

71. Lipkowitz S, Weissman AM (2011) RINGs of good and evil: RING finger ubiquitin ligases at the crossroads of tumour suppression and oncogenesis. Nat Rev Cancer 11: 629-643.

72. Gummlich L, Rabien A, Jung K, Dubiel W (2013) Deregulation of the COP9 signalosome-cullin-RING ubiquitin-ligase pathway: mechanisms and roles in urological cancers. Int J Biochem Cell Biol 45: 1327-1337.

73. Kang M, Li Y, Zhao Y, He S, Shi J (2017) miR-33a inhibits cell proliferation and invasion by targeting CAND1 in lung cancer. Clin Transl Oncol.

74. Salon C, Brambilla E, Brambilla C, Lantuejoul S, Gazzeri S, et al. (2007) Altered pattern of Cul-1 protein expression and neddylation in human lung tumours: relationships with CAND1 and cyclin E protein levels. J Pathol 213: 303-310.

75. Korzeniewski N, Hohenfellner M, Duensing S (2012) CAND1 promotes PLK4-mediated centriole overduplication and is frequently disrupted in prostate cancer. Neoplasia 14: 799-806.

76. Zhai W, Yao XD, Xu YF, Peng B, Zhang HM, et al. (2014) Transcriptome profiling of prostate tumor and matched normal samples by RNA-Seq. Eur Rev Med Pharmacol Sci 18: 1354-1360.

77. Culig Z, Hoffmann J, Erdel M, Eder IE, Hobisch A, et al. (1999) Switch from antagonist to agonist of the androgen receptor bicalutamide is associated with prostate tumour progression in a new model system. Br J Cancer 81: 242-251.

78. Hoefer J, Akbor M, Handle F, Ofer P, Puhr M, et al. (2016) Critical role of androgen receptor level in prostate cancer cell resistance to new generation antiandrogen enzalutamide. Oncotarget 7: 59781-59794.

79. Nagai T, Ibata K, Park ES, Kubota M, Mikoshiba K, et al. (2002) A variant of yellow fluorescent protein with fast and efficient maturation for cell-biological applications. Nat Biotechnol 20: 87-90.

80. Ilagan RP, Rhoades E, Gruber DF, Kao HT, Pieribone VA, et al. (2010) A new bright green-emitting fluorescent protein--engineered monomeric and dimeric forms. FEBS J 277: 1967-1978.

81. Antonov AV (2011) BioProfiling.de: analytical web portal for high-throughput cell biology. Nucleic Acids Res 39: W323-327.

82. Sboner A, Demichelis F, Calza S, Pawitan Y, Setlur SR, et al. (2010) Molecular sampling of prostate cancer: a dilemma for predicting disease progression. BMC Med Genomics 3: 8.

83. Soldani C, Scovassi AI (2002) Poly(ADP-ribose) polymerase-1 cleavage during apoptosis: an update. Apoptosis 7: 321-328.

84. Murata T, Takayama K, Katayama S, Urano T, Horie-Inoue K, et al. (2010) miR-148a is an androgen-responsive microRNA that promotes LNCaP prostate cell growth by repressing its target CAND1 expression. Prostate Cancer Prostatic Dis 13: 356-361.

85. Rulina AV, Mittler F, Obeid P, Gerbaud S, Guyon L, et al. (2016) Distinct outcomes of CRL-Nedd8 pathway inhibition reveal cancer cell plasticity. Cell Death Dis 7: e2505.

86. Chua YS, Boh BK, Ponyeam W, Hagen T (2011) Regulation of cullin RING E3 ubiquitin ligases by CAND1 in vivo. PLoS One 6: e16071.

87. Thul PJ, Akesson L, Wiking M, Mahdessian D, Geladaki A, et al. (2017) A subcellular map of the human proteome. Science 356.

88. Joseph JD, Lu N, Qian J, Sensintaffar J, Shao G, et al. (2013) A clinically relevant androgen receptor mutation confers resistance to second-generation antiandrogens enzalutamide and ARN-509. Cancer Discov 3: 1020-1029.

89. Korpal M, Korn JM, Gao X, Rakiec DP, Ruddy DA, et al. (2013) An F876L mutation in androgen receptor confers genetic and phenotypic resistance to MDV3100 (enzalutamide). Cancer Discov 3: 1030-1043.

90. Li Y, Chan SC, Brand LJ, Hwang TH, Silverstein KA, et al. (2013) Androgen receptor splice variants mediate enzalutamide resistance in castration-resistant prostate cancer cell lines. Cancer Res 73: 483-489.

91. Antonarakis ES, Lu C, Wang H, Luber B, Nakazawa M, et al. (2014) AR-V7 and resistance to enzalutamide and abiraterone in prostate cancer. N Engl J Med 371: 1028-1038.

92. Puhr M, Hoefer J, Eigentler A, Ploner C, Handle F, et al. (accepted in 2017) The glucocorticoid receptor is a key player for prostate cancer cell survival and a target for improved anti-androgen therapy. Clin Cancer Res.

93. Dozmorov MG, Hurst RE, Culkin DJ, Kropp BP, Frank MB, et al. (2009) Unique patterns of molecular profiling between human prostate cancer LNCaP and PC-3 cells. Prostate 69: 1077-1090.

94. Sampson N, Neuwirt H, Puhr M, Klocker H, Eder IE (2013) In vitro model systems to study androgen receptor signaling in prostate cancer. Endocr Relat Cancer 20: R49-64.

95. Hannus M, Beitzinger M, Engelmann JC, Weickert MT, Spang R, et al. (2014) siPools: highly complex but accurately defined siRNA pools eliminate off-target effects. Nucleic Acids Res 42: 8049-8061.

96. Bursztajn S, Feng JJ, Berman SA, Nanda A (2000) Poly (ADP-ribose) polymerase induction is an early signal of apoptosis in human neuroblastoma. Brain Res Mol Brain Res 76: 363-376.

97. Skaar JR, Pagan JK, Pagano M (2013) Mechanisms and function of substrate recruitment by F-box proteins. Nat Rev Mol Cell Biol 14: 369-381.

98. Dubiel D, Gierisch ME, Huang X, Dubiel W, Naumann M (2013) CAND1-dependent control of cullin 1-RING Ub ligases is essential for adipogenesis. Biochim Biophys Acta 1833: 1078-1084.

Curriculum Vitae

Name:	**Johanna Zwick, B.Sc.**
Address:	Ing.-Thommen-Straße 1, 6020 Innsbruck, Austria
Date of Birth:	25/09/1992
Nationality:	Austrian
Phone:	+43 681 10809700
Email:	johanna.zwick@rolmail.net
LinkedIn Profile:	https://at.linkedin.com/in/johanna-zwick-8b3453108

Academic studies

10/2015 – ongoing

Master's degree in Biochemistry and Molecular Biomedicine
Graz University of Technology (Austria)
- <u>Master thesis</u>: "The role of Cand1 in prostate cancer progression."
  A seven-months research project on the role of Cand1 protein in therapy-naive and enzalutamide-resistant prostate cancer cell lines.

10/2011 – 09/2015

Bachelor's degree in Molecular Biology
Graz University of Technology (Austria)
- <u>Bachelor thesis</u>: "Overexpression of *mscS* – a significant effect on survival?"
  A two-week research project on cloning and expression of GFP-tagged *mscS* in *E. coli* followed by growth studies.
- Receipt of a merit-based scholarship from Graz University of Technology (2013)

01/2015 – 06/2015

Erasmus+ programme: Lund University (Sweden)

09/2006 – 06/2011

Humanistisches Gymnasium „Beda Weber" (Merano, Italy)
- Receipt of school award for outstanding academic performance and social commitment (2008)

09/2009 – 06/2010

Year abroad: Bournemouth and Poole College (England)
- General Certificate of Education - Advanced Subsidiary (AS) level

Practical Trainings

03/2017 – 10/2017

Master's thesis on prostate cancer
Department of Urology, Medical University of Innsbruck (Austria)

07/2016 – 08/2016	**Research project on dendritic cells**
	Department of Dermatology, Innsbruck University Hospital (Austria)
08/2015	**Internship in the laboratory for medical microbiology**
	Merano Hospital (Italy)
08/2014 and	**Internship in quality management in food industry**
07/2013 – 08/2013	Dr. Schär (Postal, Italy)

Additional Skills and Interests

Further education:	Participation and short talk at the 1st Translational Science Meeting 2017 in Innsbruck (20. – 21. October 2017)
	Participation at the annual ÖGMBT meeting in Innsbruck (25. – 27. September 2017)
	Project management – Communicating Science
	Introduction to Business Administration – TIMEGATE (Transfer Initiative for Management- and Entrepreneurship basics, Awareness, Training and Employability)
Languages:	German – native speaker
	Italian – bilingual proficiency (C2) – Certificate of Bilingualism A
	English – professional working proficiency (C2)
	French – limited working proficiency (B1)
	Swedish – elementary proficiency (A2)
Computer skills:	MS Office Applications (Word, PowerPoint, Excel) incl. European Computer Driving Licence (ECDL) and Touch Typing
Voluntary work:	Board member and chairwoman of the South Tyrolean Student's Union in Graz (2012 – 2014)
	▪ Giving advice and support to students regarding studying and major issues facing universities
	▪ Organizing cultural and social events in order to facilitate regular communication and social networking
	Class representative at secondary school (2006 – 2008)
Sports involvement:	Volleyball player at Sportclub Meran (SCM) and Associazione sportiva di Merano (ASM) including participation in championships and tournaments (2003 – 2009)

Innsbruck, 20th November 2017

Abstract presented at the 1st Translational Science Meeting 2017 in Innsbruck:

Low Cand1 expression is associated with reduced prostate cancer growth

Johanna Zwick, Andrea Eigentler, Julia Hoefer, Martin Puhr, Helmut Klocker*, Isabel Heidegger*

Department of Urology, Division of Experimental Urology, Medical University of Innsbruck, Austria

* Equally contributing senior authors

Background Prostate cancer (PCa) is one of the most common cancers in men of developed countries. Evidence has accumulated showing the importance of cullin-RING ubiquitin ligases (CRLs) and their regulator Cand1 in various cancer entities. In the present study, we analysed the impact of Cand1 in PCa. In this context, we also elucidated the role of Cand1 in PCa cell lines resistant to the androgen receptor inhibiting agent enzalutamide, as we previously discovered that Cand1 might be involved in resistance mechanisms.

Material and Methods Using a pool of four targeting siRNAs, we downregulated Cand1 in the metastatic PCa cell lines LNCaP and PC3, as well as in LAPC-4 and LNCaP abl cells resistant to enzalutamide (EnzaR). Effects on cell viability, proliferation and apoptosis were examined employing WST-1 cell viability-, ^{3}H-thymidine incorporation assay, measurement of cPARP levels (Western blot) and caspase 3/7 activity, respectively. BioProfiling, a gene expression data mining database was used for validation of expression in PCa.

Results Knockdown of Cand1 significantly reduced cell viability and proliferation in LNCaP and PC3 cells and resulted in an increased apoptosis. The same effects were observed in EnzaR cells, however, less pronounced compared to the respective treatment-naive cell lines. Using the BioProfiling database we were able to show that low Cand1 expression is associated with increased overall survival in PCa patients.

Conclusion Interim results of this study indicate that Cand1 expression modulates proliferation and survival of hormone-therapy-naive as well as enzalutamide-resistant cell lines. Moreover, Cand1 levels seem to correlate with overall survival rates in PCa patients. We propose further investigations on Cand1 in order to reveal its impact on PCa progression and its potential involvement in enzalutamide resistance.